

Dexterous Robotic Cutting Based on Fracture Mechanics and Force Control

Xiaoqian Mu, Yuechuan Xue, and Yan-Bin Jia

Abstract—Skills of cutting natural foods are important for robots looking to play a bigger role in kitchen assistance. The basic objective of cutting is to achieve material fracture via smooth movements of a kitchen knife, which in the process performs work to overcome material toughness, acts against blade-material friction, and generates shape deformation. This paper investigates how a robotic arm drives the knife to cut through an object in a sequence of three moves: pressing, touching, and slicing. To cope with evolving contacts with the material and cutting board, position, force, and impedance controls act either separately or jointly, assisted by force sensing and/or based on fracture mechanics, so the knife follows a prescribed trajectory to split the object. Force data acquired during the phase of pressing are used for estimating the object-specific values of physical parameters related to cutting. These estimated values are promptly used for control purpose to execute the phase of slicing. Experiments over several types of fruits and vegetables have exhibited natural cutting movements like those performed by a human hand.

Note to Practitioners—Automation of kitchen skills is an important step in the development of home robots, which are expected to relieve us from daily chores and help us care for the elderly and people with disabilities. The motivation of this research is to enable a robotic arm to cut natural foods with knife movements that bear the smoothness and efficiency of those executed by a human hand. Existing methods on robotic cutting have focused on force control to ensure material separation but not on execution of natural knife movements. This paper dissects a cutting action into three phases, as inspired from the human hand execution, and realizes them via different control policies. These policies are based on sensing and modeling the forces experienced by the knife through its interactions with the material and the cutting board. Preliminary experimental results have demonstrated cutting of various food items with speed and smoothness. In future research, we will address cutting of deformable objects and explore issues including energy efficiency, cutting by the knife held in a robotic hand, and food stabilization and manipulation by a second arm/hand.

Index Terms—Dexterous cutting, fracture mechanics, force control, knife skills, real-time material property estimation.

I. INTRODUCTION

AUTOMATION of kitchen skills is an important step towards the advent of multipurpose home robots, which have long been a public fascination. Robot assistance in the kitchen will improve the life quality of people by saving

their time on meal preparation. It will also relieve the elderly and people with disabilities from the tedious task and allow them needed rest. Until today, such assistance has been mostly limited to peripheral tasks such as washing and sorting dishes [1], carrying food trays [2], and making pancakes and noodles [3], burgers [4], etc., out of prepared raw materials in very structured settings [5]. Robots can play a bigger role in the kitchen by becoming more versatile.

Robotic food manipulation [6], [7], not limited to food grasping [8], feeding [9], cooking [10], etc., has attracted increasing attention. Food cutting, an integral part of automatic meal preparation, stands out as one of the ultimate tests on human-level dexterity for robots, which today still lack basic knife skills such as chop, slice, and dice. Here, a robot is expected to use the same kitchen knife to cut a variety of raw foods including fruits, vegetables, and meats. This is very different from in the food industry, where every robot is capable of only one task, whether cutting meat [11], deboning [12], or butchering chicken [13]. Efficiency in the industry also benefits from the use of specially designed tools for slicing or holding foods [14]. Likewise, in the everyday life, specialized kitchen tools sold at stores or online [15] to cut French fries, slice lettuce and tomatoes, peel potatoes, chop fruits and vegetables, and so on. To automate meal preparation at home without a robotic hand possessing cutting skills would require a large collection of such specialized machines. This would be unrealistic given the high cost and limited kitchen space, and also inefficient and clumsy due to constant switches among the cutting machines.

Can a robot cut various raw foods in natural and smooth actions as the human hand does? The main technical challenge is to plan and control the movement of the held knife through a material while reacting to forces of different natures (fracture, friction, tension, viscosity, and contact) that are exerted by the material and cutting board, just like a knife-holding human hand feels them during a cutting action. Knowledge about the forces of fracture and tension (and consequently that of blade-material friction) can be used to dynamically adjust the cutting trajectory to reduce the effort or deformation of the object. Estimates of the contact force between the knife and the cutting board can help control the knife to slice through the object while pressing on the board to ensure a full separation of the material. Unfortunately, these forces cannot be separately estimated via force sensing alone. Some modeling therefore is needed. Elasticity theories [16], [17] and fracture mechanics [18] can be drawn upon for this purpose.

Unlike other robotic manipulation tasks, the objective of cutting is to alter the structure of the manipulated object.

*Support for this research was provided by the US National Science Foundation under Grant IIS-1651792. Any opinions, findings, and conclusions or recommendations expressed in this material are those of the authors and do not necessarily reflect the views of the National Science Foundation.

Xiaoqian Mu is with Aescape Inc., New York, NY 10011, USA (e-mail: xqmu1005@gmail.com).

Yuechuan Xue is with Amazon, Cambridge, MA 02142, USA (e-mail: yuechxue@amazon.com).

Yan-Bin Jia is with the Department of Computer Science, Iowa State University, Ames, IA 50011, USA (e-mail: jia@iastate.edu).

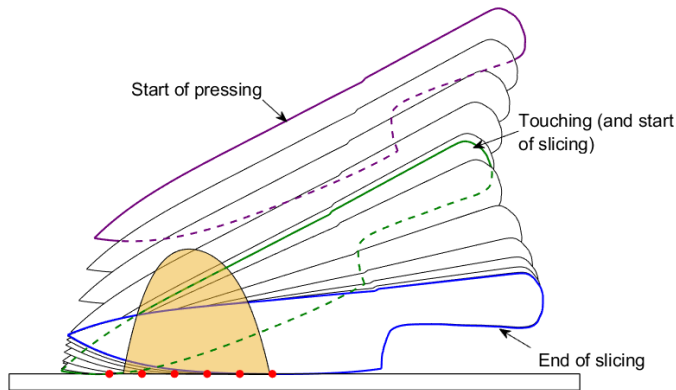


Fig. 1. Three phases of cutting: pressing, touching, and slicing. The knife poses, drawn in purple, green, and blue, respectively mark the beginnings of pressing and touching, and the end of slicing. Also drawn are the visible contours of some intermediate poses. The red dots on the cutting board mark several intermediate positions of the contact point between the knife’s edge and the board as the object is being cut open.

Whereas in most manipulation tasks only one object is handled at a time, in cutting two objects are simultaneously manipulated: the knife and the food item. To achieve a full scale of dexterity in robotic cutting, the research community needs to resolve a host of issues, from fracture modeling, to knife holding and control, to object stabilization and maneuver, and to coordination of two hands/arms. We intend to take up these challenges one at a time with increasing complexities for years to come.

As a first step, this paper investigates a cutting task executed by a knife, rigidly attached to a robotic arm, on a cutting board. We draw inspirations from skillful cutting by the human hand. One common way of cutting is to move the knife downward against the cutting board, and upon contact, pull its edge on the board to slice the item into two pieces. This has motivated us to decompose the cutting action into three consecutive phases (illustrated in Fig. 1): *pressing*, in which the knife moves fast downward along a prescribed trajectory until its edge makes contact with the cutting board; *touching*, in which the knife softens its impact on the board; and *slicing*, in which the knife separates the object completely with its edge sliding/rolling on the board across the object’s bottom.

Skillful cutting is often evidenced from precision and speed. The robotic arm is expected to move the knife swiftly. For this reason, cutting is not treated as a quasi-static manipulation in which the manipulated object typically moves at a low speed, the inertial force is negligible, and the dissipative forces are parallel to the object’s velocity and of constant magnitude [19].¹ The food item, meanwhile, barely moves (except for deforming and fracturing) regardless of the force exerted on it by the knife. Cutting is thus not a dynamic manipulation in the usual sense since the food item is subjected to negligible inertial force.

¹Also, in quasi-static manipulation, feedback control is conducted in an ad hoc manner because it is the velocity of the robotic arm, not its exerted force/torque, which would be used for adjusting the object’s velocity [20].

Based on the dynamics of the robotic arm and the quasi-static interaction between the “motionless” object and the knife, this paper seeks to resolve several key issues of cutting that include path following, impact handling, and force regulation. The goal is steady progress leading up to a complete separation of the object into two pieces. The three phases of cutting, partitioned so according to changing contacts and path constraints, are carried out under position control, hybrid position/impedance control, and hybrid position/force control, respectively.

A. Contributions and Outline of the Article

Our work on cutting to be presented bears a number of distinct characteristics and technical novelties:

- 1) It investigates an under-researched form of manipulation which alters the structure of the manipulated object in the process.
- 2) It decomposes a complex maneuver (of a kitchen knife) into multiple phases (pressing, touching, and slicing), and carries them out under different control policies.
- 3) To realize slicing, fracture mechanics are used for modeling the forces due to fracture and friction in order to regulate the knife’s contact with the cutting board.
- 4) The values of physical parameters estimated in the initial pressing phase of cutting are promptly used for modeling to control the knife movement in the ending slicing phase. This robustly deals with variations of these values among natural objects especially foods, even of the same type, in the interior of the same object, and due to its gradual loss of freshness.
- 5) Cutting experiments are performed on fruits and vegetables (rather than on synthetic objects as often studied in fracture mechanics).

The rest of the paper is organized as follows. Section I-B presents the notation used in the paper. Section II reviews works in related areas including fracture mechanics and various genres of cutting: graphics-oriented, surgery-intended, control-based, and data-driven. Section III formulates the technical problem of cutting and presents its underlying mechanics. Section IV focuses on cutting control of a robotic arm, which has n degrees of freedom (DOFs) in the cutting plane, to adjust to changing contact situations. Section V tackles real-time estimation of physical parameters including fracture toughness, pressure distribution, and coefficient of friction for an object as it is being cut open. Section VI describes experiments conducted on cutting fruits and vegetables with a 4-DOF WAM Arm utilizing its two DOFs in a vertical plane. Discussion and future work follow in Section VII.

This paper extends an earlier conference version [21] in several aspects. First, it generalizes the cutting scheme to a robotic arm with more than two DOFs in the cutting plane. In the pressing phase, the knife’s orientation is now controlled directly, rather than realized via a constraint, to allow more flexibility of cutting and also to simplify control. In the touching phase, impedance control is added to lessen the impact between the knife and the cutting board. Second, inverse kinematics is no longer needed in the hybrid position/force

TABLE I
NOMENCLATURE.

\cdot	Differentiation with respect to time.	\mathbf{f}_F	Force due to blade-material friction.
\top	Transpose of matrix.	\mathbf{f}_S	Force reading by an F/T sensor at \mathbf{a} .
\mathcal{W}	World frame.	τ_C	Torque on \mathbf{a} due to fracture.
\mathcal{A}	Arm frame.	τ_F	Torque on \mathbf{a} due to friction.
\mathcal{K}	Knife frame.	$\boldsymbol{\tau}$	Arm's joint torque vector.
\mathbf{o}	Origin of \mathcal{W} .	M	Combined inertia matrix of arm, sensor, and knife.
\mathbf{a}	Arm's open end (origin of \mathcal{A}).	C	Combined Coriolis matrix.
\mathbf{p}	Knife's tip point (origin of \mathcal{K}).	N	Combined gravity term.
ϕ	Rotation of \mathcal{A} from \mathcal{W} .	$\boldsymbol{\rho}_a$	Wrench exerted at \mathbf{a} .
ψ	Rotation of \mathcal{K} from \mathcal{W} .	$\boldsymbol{\tau}_a$	Combined torque due to Coriolis, centrifugal, gravitational, and external forces at \mathbf{a} .
θ_i	Arm's i th joint angle.	J_a	Jacobian at \mathbf{a} (w.r.t. $\boldsymbol{\theta}$).
$\boldsymbol{\theta}$	Arm's joint angle vector.	\mathbf{c}	Knife-board contact (lowest point on β_θ).
ω	Knife's angular velocity.	$\boldsymbol{\tau}_c$	Combined torque due to Coriolis, centrifugal, gravitational, and external forces at \mathbf{c} .
β'	Knife's edge curve in \mathcal{K} .	J_c	Jacobian at \mathbf{c} (as fixed on knife's edge).
γ'	Knife's spine curve in \mathcal{K} .	$k_{p a}, k_{i a}, k_{v a}$	Proportional, integral and derivative gains for position control during pressing, where \mathbf{a} is the point of interest.
β_θ	Knife's edge curve in \mathcal{W} .	k_r, d_r, b_r	Desired stiffness, damping and mass for impedance control during touching.
γ_θ	Knife's spine curve in \mathcal{W} .	$k_{p c}, k_{i c}, k_{v c}$	Proportional, integral and derivative gains for position control during slicing, where \mathbf{c} is the point of interest.
σ	Object's contour curve in the cutting plane.	k_{fi}	Integral gain for contact force control.
κ	Object's fracture toughness.		
μ	Coefficient of blade-object friction.		
P	Pressure distribution of blade-object contact.		
Ω	Region of blade-object contact.		
\mathbf{f}_C	Fracture force.		

controller for the slicing phase. Third, the parameters of fracture and friction that were measured before experiments are now estimated on the fly and more accurately for the object. Finally, we have conducted more extensive simulation and experiments, with an added demonstration of chopping.

B. Notation

In this paper, a vector is represented by a lowercase letter in bold, e.g., $\mathbf{a} = (a_x, a_y)^\top$, with its x - and y -coordinates denoted by the same (non-bold) letter with subscripts x and y , respectively. A unit vector has a hat, e.g., $\hat{\mathbf{a}} = \mathbf{a}/\|\mathbf{a}\|$. The cross product $\mathbf{a} \times \mathbf{b}$ of two tuples \mathbf{a} and \mathbf{b} is treated as a scalar. The subscripts d and e refer to the desired value and error, respectively. For example, a_{yd} and a_{ye} are respectively the desired value for and error in a_y . A matrix is denoted by an upper case letter, e.g., A , and its pseudo-inverse by the superscript \dagger , e.g., A^\dagger . We denote a submatrix of A as \bar{A} . Table I summarizes the notation for geometry, mechanics, and control as used in the paper.

II. RELATED WORK

This research draws upon fracture mechanics for both modeling of a cutting action and force control in its implementation with a robot. Cutting has been studied in mechanics through analysis, in graphics with pure simulation purpose, and for surgical training and assistance. Most strategies for robotic cutting are either control-based or data-driven.

A. Fracture Mechanics

Fracture mechanics [22] builds on a balance between the work done by the knife and the total amount spent on crack propagation, transformed into other energy forms (strain, kinetic, chemical, etc.), and dissipated by friction. Methods for measuring the cutting force and fracture toughness were

studied for ductile materials [23] and live tissues [24], [25]. Fracture force and torque could be obtained via integration along the knife's edge [26]. In this paper, such approach has been extended to also account for the blade-material friction in modeling. A "slice-push ratio" introduced in [27] quantified the amounts of work done along two orthogonal directions in an effort to characterize the dramatic decrease in the fracture force when the knife was performing a sideways slicing motion. A different explanation [28] for such decrease stated that pressing caused global deformation while slicing yielded local deformation (and thus required less effort to create fracture). A recent analysis [29] derived a closed form for the change in fracture toughness in terms of the slice-push ratio and Poisson's ratio of the material only.

B. Cutting in Graphics

Cutting of deformable objects has been simulated in the field of graphics using either mesh-based or mesh-free methods. Employing a state machine, a real-time algorithm [30] processed plane intersections within a tetrahedral mesh with the objective of surgical cutting simulation. A virtual node algorithm [31] allowed a mesh to be cut along any piecewise linear path by replicating fractured elements. In [32], simulation of surgical cutting was conducted using a mesh-free method based on dynamics to provide force feedback in the real time. The material point method, a hybrid of mesh-free and mesh-based methods, dynamically simulated fracture of various materials with high visual fidelity [33].

C. Surgical Cutting

Surgical training makes use of realistic haptic display of soft tissue cutting. Supported by simulation, the stress distribution within a biomaterial during cutting was analyzed in [34] and the resulting force of cutting was calculated and verified

via the the finite element method (FEM) and experiment in [35]. In [36], the force to realize compression cutting of a biomaterial was predicted based on its property and the knife’s sharpness. Haptic models, mostly empirical, were developed for animal tissue cutting with a pair of scissors [37], soft tissue deformation prior to fracture [38], as well as needle insertion² into soft tissues [40]. In surgical pattern cutting with a pair of scissors, a policy of tension (for the second tool) which consisted of a sequence of pinch points and their displacements, was generated using deep reinforcement learning [41]. To improve safety in robot-assisted laminectomy, the cutting depth was monitored based on the modeled and sensed milling forces with a high accuracy [42]. In [43], cutting of a biological tissue was realized as vision-guided and modeling-based dynamic tracking of the knife’s depth into the tissue in its original state. We refer to [44] for a survey on mechanics and modeling of cutting biological materials.

D. Control-Based Cutting

Robotic cutting has been investigated in a number of ways: learning of the applied force under adaptive control based on position and velocity histories [45], adaptive force tracking via impedance control [46], visual servoing coupled with force control [47], and cooperation between cutting and pulling robots by regulating impedance [48]. A 2-DOF robot [49] was even able to debone a bird by following some cutting path constructed from x-ray imaging based on force feedback, with the help from a passive fixation mechanism. An optical multimodal-sensing skin [50] for the robotic gripper was developed to prevent unexpected motions of the knife when cutting vegetables.

Cutting is usually carried out with the knife following a trajectory through contact between its blade and the material, and often, also between its edge and the cutting board. Due to the varying nature of contact experienced by the knife in the course of a cutting action, it would be natural to employ multiple control policies. Position control [51, pp. 190-199] can realize trajectory following during the pressing phase of our cutting scheme (see Fig. 1); impedance control [52], [53], which adjusts the contact force from a motion deviation like some intended mass-spring-damper, is suitable for the touching phase to reduce the impact between the knife and cutting board caused by a fast downward knife movement; and hybrid control [54], [55], which simultaneously regulates position and force in orthogonal directions, is a default choice for the slicing phase, during which the knife’s edge moves on the cutting board. In order for the entire action of cutting to look natural, smooth transitions between these policies would be desirable, similar to a switch between position and force controls to regulate the contact force during an impact [56]. To deal with contact constraints, controls of force and position are more effectively conducted in the work space [57] using a reduced set of coordinates [58, pp. 501–510].

²Early work [39] investigated piercing.

E. Data-Driven Food Cutting

Artificial intelligence and machine learning have also been applied in cutting, with data-driven approaches becoming an active research topic. In [59], haptic data acquired during cutting were used to extract, via supervised learning, physical properties such as hardness, elasticity, and adhesiveness of the material. In [60], “dynamics” of cutting, modeled as the change in the knife position due to the applied force, was learned using a deep neural network and applied under model predictive control [61] to food cutting. This approach to cutting was later extended in [62] and [63], with force data incorporated and dynamics modeled using a recurrent neural network. A system was developed in [64] to learn the type of the object from vibrations and force/torque readings and then generate a motion to slice the object open. In [65], parameters for mesh-based simulation of robotic cutting of soft materials were learned over force profiles from real cutting scenarios using a model that combined FEM, virtual nodes, and linear springs (across the cutting plane). In [66], grapefruit cutting was achieved using a closed-loop position controller with desired trajectory generated based on a pulp and peel classifier trained over measured joint torques. Recently, a learning-based system was proposed in [67] for cutting multi-material (rigid core and soft outer layer) objects, employing an adaptive policy based on the estimated core geometry and allowable variations to optimize material cut-off ratio, reduce collision, and minimize energy consumption.

III. MECHANICS OF CUTTING

In this section, we present the geometry of the cutting task, and analyze different forces encountered by the knife as it creates fracture. To concentrate on knife skill realization, we make the following four assumptions throughout the paper:

- (A1) The object being cut deforms negligibly.
- (A2) The object remains stable during cutting.
- (A3) The knife moves in a vertical plane.
- (A4) The knife’s blade has negligible thickness.

The first assumption arises from that some vegetables and fruits such as potatoes, onions, and apples barely deform during cutting. The second assumption can be realized by having the object fixed or held by a robotic hand. The third assumption reflects the most common way of cutting in the kitchen by the human. The fourth one is reasonable since a kitchen knife’s blade typically has thickness in the range 0.4 – 2.0 mm from edge to spine.

A. Task Geometry

As shown in Fig. 2, cutting of an object takes place in the vertical x - y plane, referred to as the *world frame* \mathcal{W} , which is located at some point \mathbf{o} on the cutting board. The knife is rigidly mounted on the open end \mathbf{a} of a robotic arm whose base is located at \mathbf{b} . Both the knife and arm as modeled lie and move in the x - y plane. The arm has n (≥ 3) revolute joints with angles $\theta_1, \theta_2, \dots, \theta_n$ to actuate n links with lengths l_1, l_2, \dots, l_n , respectively. All the joint angles form a vector

$$\boldsymbol{\theta} = (\theta_1, \theta_2, \dots, \theta_n)^\top.$$

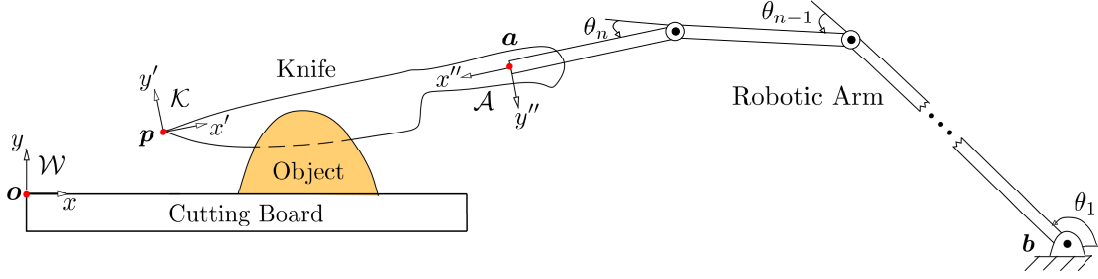


Fig. 2. n -DOF planar robotic arm cutting an object.

The arm's open end is at

$$\mathbf{a}(\boldsymbol{\theta}) = \begin{pmatrix} a_x \\ a_y \end{pmatrix} = \mathbf{b} + \sum_{i=1}^n l_i \begin{pmatrix} \cos(\sum_{j=1}^i \theta_j) \\ \sin(\sum_{j=1}^i \theta_j) \end{pmatrix}, \quad (1)$$

where the *arm frame* \mathcal{A} with x'' - and y'' -axes is located. This frame rotates through an angle

$$\phi = \theta_1 + \theta_2 + \dots + \theta_n \quad (2)$$

from the world frame \mathcal{W} . Since the knife is rigidly connected to the arm's open end, its point in the frame \mathcal{A} has the fixed position \mathbf{p}'' and in the world frame \mathcal{W} has the position

$$\mathbf{p}(\boldsymbol{\theta}) = \mathbf{a}(\boldsymbol{\theta}) + R(\phi)\mathbf{p}''. \quad (3)$$

Here

$$R(\phi) = \begin{pmatrix} \cos \phi & -\sin \phi \\ \sin \phi & \cos \phi \end{pmatrix}$$

describes the rotation of \mathcal{A} from \mathcal{W} . Attached to the point \mathbf{p} is the *knife frame* \mathcal{K} with x' - and y' -axes. This frame rotates from the frame \mathcal{A} through a constant angle ψ_0 , and thus from the frame \mathcal{W} through

$$\psi = \phi + \psi_0. \quad (4)$$

The shapes of kitchen knives differ by culture. Some have straight edges and spines, while others have curved ones. The kitchen knife considered here has both curved edge and spine, in part because knives of this type are quite common, and in part because straight edge and spine can be considered as degenerate cases of curved ones. As depicted in Fig. 3, the knife's edge and spine are described in the knife frame \mathcal{K} by two curves $\boldsymbol{\beta}'(u) = (\beta'_x, \beta'_y)^\top$ and $\boldsymbol{\gamma}'(q) = (\gamma'_x, \gamma'_y)^\top$, respectively, such that $\boldsymbol{\beta}'(0)$ and $\boldsymbol{\gamma}'(0)$ coincide with the frame's origin at the knife point \mathbf{p} . In the world frame \mathcal{W} , they are thus described by the following two curves:

$$\begin{aligned} \boldsymbol{\beta}_\theta(u) &= \mathbf{p} + R(\psi)\boldsymbol{\beta}'(u), \\ \boldsymbol{\gamma}_\theta(q) &= \mathbf{p} + R(\psi)\boldsymbol{\gamma}'(q). \end{aligned} \quad (5)$$

These two curves, each with three degrees of freedom as a part of the knife, depend on $\boldsymbol{\theta}$, which determines \mathbf{p} and ψ according to (2)–(4). More specifically, they are from two families of curves parameterized with $\boldsymbol{\theta}$ but generated respectively from $\boldsymbol{\beta}'$ and $\boldsymbol{\gamma}'$. Substituting (3) into (5), we obtain

$$\boldsymbol{\beta}_\theta(u) = \begin{pmatrix} \beta_{\theta,x}(u) \\ \beta_{\theta,y}(u) \end{pmatrix} = \mathbf{a}(\boldsymbol{\theta}) + R(\phi)\mathbf{p}'' + R(\psi)\boldsymbol{\beta}'(u). \quad (6)$$

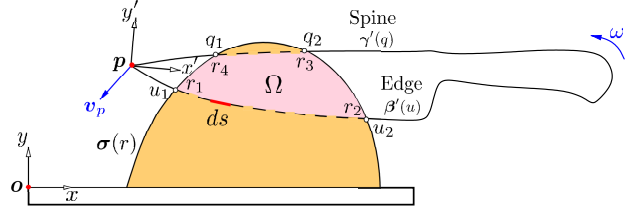


Fig. 3. Geometry of cutting.

When $\boldsymbol{\theta}$ is allowed to vary, $\boldsymbol{\beta}_\theta$ is a function with $n+1$ variables $\theta_1, \theta_2, \dots, \theta_n$, and u .

As cutting proceeds, the knife's edge intersects the object at a section of $\boldsymbol{\beta}_\theta(u)$ over some interval $[u_1, u_2]$, $u_1 \leq u_2$, as illustrated in Fig. 3. The section is denoted $\boldsymbol{\beta}_\theta[u_1, u_2]$ for convenience. A section $\boldsymbol{\gamma}_\theta[q_1, q_2]$ of the spine $\boldsymbol{\gamma}_\theta(q)$ over $[q_1, q_2]$, for some q_1 and q_2 , may also be inside the object.

Since the object does not deform under assumption A1, we let the curve $\boldsymbol{\sigma}(r)$ describe the non-varying contour of its cross section intersected by the x - y plane. The knife's edge intersects the curve at $\boldsymbol{\sigma}(r_1)$ and $\boldsymbol{\sigma}(r_2)$ from left to right. Thus,

$$\begin{aligned} \boldsymbol{\beta}_\theta(u_1) &= \boldsymbol{\sigma}(r_1), \\ \boldsymbol{\beta}_\theta(u_2) &= \boldsymbol{\sigma}(r_2). \end{aligned}$$

The segments $\boldsymbol{\beta}_\theta[u_1, u_2]$ and $\boldsymbol{\sigma}[r_2, r_1]$ enclose the region of fracture. When a section of the spine $\boldsymbol{\gamma}_\theta[q_1, q_2]$ is inside the cross section, it is bounded by $\boldsymbol{\sigma}(r_4)$ and $\boldsymbol{\sigma}(r_3)$ such that

$$\begin{aligned} \boldsymbol{\gamma}_\theta(q_1) &= \boldsymbol{\sigma}(r_4), \\ \boldsymbol{\gamma}_\theta(q_2) &= \boldsymbol{\sigma}(r_3). \end{aligned}$$

The four segments $\boldsymbol{\beta}_\theta[u_1, u_2]$, $\boldsymbol{\sigma}[r_2, r_3]$, $\boldsymbol{\gamma}_\theta[q_1, q_2]$, and $\boldsymbol{\sigma}[r_4, r_1]$ bound the region Ω of contact between the blade and the object.

B. Forces During Cutting

New fracture is being created by the edge segment $\boldsymbol{\beta}_\theta[u_1, u_2]$, which is experiencing a force \mathbf{f}_C due to material fracture. In other words, the work done by $-\mathbf{f}_C$ is yielding fracture. Meanwhile, the blade is experiencing a force \mathbf{f}_F due to its friction with the object's material inside the contact region Ω . If the object were deformable, the force exerted by the knife would have a third component $-\mathbf{f}_U$ that does work to cause an increase (or decrease) of the object's strain energy. Under assumption A1, however, we have $\mathbf{f}_U = \mathbf{0}$.

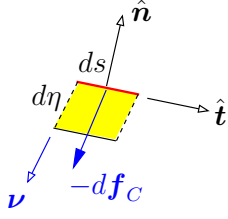


Fig. 4. Area of fracture yielded by an element of length ds on the knife's edge.

Consider an infinitesimal element of length ds on the knife's edge starting at $u \in [u_1, u_2)$. See Fig. 4. The element may or may not be generating fracture due to the knife's rotation. Since the latter case is easy to check from the element's instantaneous motion, we need only consider the former case here. Let $\omega = \dot{\theta}_1 + \dot{\theta}_2 + \dots + \dot{\theta}_n$ be the knife's angular velocity. The element exerts the force $-df_C$ in the direction of its velocity $\nu = d\beta_\theta/dt$, obtained from differentiating (6) as

$$\begin{aligned} \nu &= \dot{\mathbf{a}} + \frac{d}{dt}(R(\phi))\mathbf{p}'' + \frac{d}{dt}(R(\psi))\beta' \\ &= \dot{\mathbf{a}} + \omega R(\phi) \begin{pmatrix} -p_x'' \\ p_y'' \end{pmatrix} + \omega R(\psi) \begin{pmatrix} -\beta_x' \\ \beta_y' \end{pmatrix}. \end{aligned}$$

A movement by the element over distance $d\eta$ generates an area of fracture that is a parallelogram (shown in Fig. 4). Its four sides are parallel to either the edge tangent

$$\hat{\mathbf{t}} = \left(\frac{\partial \beta_{\theta,x}}{\partial u}, \frac{\partial \beta_{\theta,y}}{\partial u} \right)^\top / \left\| \left(\frac{\partial \beta_{\theta,x}}{\partial u}, \frac{\partial \beta_{\theta,y}}{\partial u} \right)^\top \right\|$$

or the velocity ν . Now we make use of the material's *fracture toughness* κ , which is defined to be the energy required to propagate a crack by unit area [22, p. 16]. The work done by $-df_C$ over the movement is equal to the energy needed for creating the parallelogram of fracture:

$$(-df_C \cdot \hat{\nu})d\eta = -\kappa(\hat{\nu} \cdot \hat{\mathbf{n}})d\eta ds,$$

where $\hat{\nu} = \nu/\|\nu\|$ and $\hat{\mathbf{n}}$ is the unit inward normal at $\beta_\theta(u)$. From the above and that df_C and $\hat{\nu}$ are collinear, we obtain

$$\begin{aligned} df_C &= \kappa(\hat{\nu} \cdot \hat{\mathbf{n}})\hat{\nu} ds \\ &= \kappa \left(\hat{\nu} \cdot \left(-\frac{\partial \beta_{\theta,y}}{\partial u}, \frac{\partial \beta_{\theta,x}}{\partial u} \right)^\top \right) \hat{\nu} du. \end{aligned} \quad (7)$$

Integration over the segment $S = \beta_\theta[u_1, u_2]$ yields the total fracture force:

$$\mathbf{f}_C = \int_S df_C. \quad (8)$$

Since the knife is rigidly attached to the robotic arm's open end \mathbf{a} , the fracture force yields a torque at the point:

$$\tau_C = \int_S (\beta_\theta(u) - \mathbf{a}) \times d\mathbf{f}_C. \quad (9)$$

Coulomb friction is assumed inside the contact region Ω on both sides of the blade. Let the unit vector $\hat{\nu}(x, y)$ denote the direction of the velocity of an area element at $(x, y)^\top \in \Omega$. Since both sides of the blade is subject to friction, the force received at the open end \mathbf{a} is

$$\mathbf{f}_F = -2\mu \iint_\Omega P(x, y)\hat{\nu} dx dy, \quad (10)$$

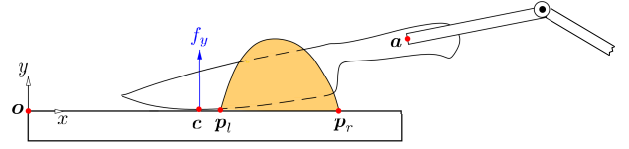


Fig. 5. Knife in contact with the cutting board.

where μ is the coefficient of friction and $P(x, y)$ is the pressure distribution of the blade at $(x, y)^\top$. Similarly, the torque at \mathbf{a} due to friction is

$$\tau_F = -2\mu \iint_\Omega P(x, y) \left(\begin{pmatrix} x \\ y \end{pmatrix} - \mathbf{a} \right) \times \hat{\nu} dx dy. \quad (11)$$

The wrenches $(\mathbf{f}_C, \tau_C)^\top$ and $(\mathbf{f}_F, \tau_F)^\top$ can be evaluated given the knife's pose $(\mathbf{p}^\top, \psi)^\top$ and velocities $(\mathbf{v}_p^\top, \omega)^\top$, where \mathbf{v}_p is the velocity of the knife point. If the knife is translating and $P(x, y)$ has uniform distribution, they have simple forms that are derived in Appendix A. In the general case, the points on the blade within the region Ω do not have the same velocity, which implies that the fracture and frictional forces and torques can only be calculated numerically.

Subtracting the wrench

$$\rho_K = \begin{pmatrix} \mathbf{f}_C + \mathbf{f}_F \\ \tau_C + \tau_F \end{pmatrix} \quad (12)$$

from the reading $(\mathbf{f}_S, \tau_S)^\top$ of a force/torque sensor³ located at \mathbf{a} after compensating for the gravitational effects of the sensor and knife, we will be able to determine forces of other sources, in particular, the contact force between the knife and the cutting board. This information will be used later for knife control during the last phase of cutting in Section IV-C.

IV. CONTROL OF CUTTING BY A PLANAR ARM

Cutting of an object proceeds in three phases that were previously illustrated in Fig. 1. The first phase is *pressing*, during which the arm translates the knife downward until its edge contacts the cutting board. The second phase, transitional, is *touching*, during which the arm quickly slows down the knife's vertical motion to soften its contact with the board. The third phase is *slicing*, during which the arm translates and rotates the knife to move its contact point with the cutting board across the object's bottom segment $\overline{p_l p_r}$ (see Fig. 5) in the cutting plane. By now the object has been split into two parts. In this section, we describe control strategies for carrying out the above three phases of cutting.

The arm frame \mathcal{A} has generalized coordinates

$$\mathbf{x} = (a_x, a_y, \phi)^\top, \quad (13)$$

which has the derivative

$$\dot{\mathbf{x}} = J_a \dot{\boldsymbol{\theta}}, \quad (14)$$

where

$$J_a = \frac{\partial \mathbf{x}}{\partial \boldsymbol{\theta}} \quad (15)$$

is a $3 \times n$ Jacobian matrix derived from (1) and (2).

³In the implementation, the sensor rigidly connects the open end and the knife with \mathbf{a} chosen as the sensor's center.

The kitchen knife, driven by the n -DOF arm ($n \geq 3$), can follow any given trajectory in the cutting plane (as long as no joint limit is exceeded). Since both the F/T sensor and the knife are rigidly mounted on the arm, they are treated as parts of the arm's distal link. The arm dynamics in the joint space is given as follows:

$$\boldsymbol{\tau} = M(\boldsymbol{\theta})\ddot{\boldsymbol{\theta}} + C(\boldsymbol{\theta}, \dot{\boldsymbol{\theta}})\dot{\boldsymbol{\theta}} + N(\boldsymbol{\theta}) - J_a^\top \boldsymbol{\rho}_a, \quad (16)$$

where $\boldsymbol{\tau}$ is the arm's joint torque vector, $M(\boldsymbol{\theta})$ is an $n \times n$ mass matrix accounting for the sensor and knife, $C(\boldsymbol{\theta}, \dot{\boldsymbol{\theta}})\dot{\boldsymbol{\theta}}$ includes the Coriolis and centrifugal terms, $N(\boldsymbol{\theta})$ is the gravity term⁴, and $\boldsymbol{\rho}_a$ is the wrench (force and torque) exerted at the arm's open end \boldsymbol{a} due to the knife's interactions with the object and the cutting board.

Assuming that J_a has full row rank, we obtain the joint acceleration from differentiating equation (14):

$$\ddot{\boldsymbol{\theta}} = J_a^\dagger (\ddot{\boldsymbol{x}} - \dot{J}_a \dot{\boldsymbol{\theta}}), \quad (17)$$

where

$$J_a^\dagger = J_a^\top (J_a J_a^\top)^{-1} \quad (18)$$

is the Moore-Penrose inverse [68] of J_a .⁵ The arm dynamics (16) can be rewritten in the task space:

$$\boldsymbol{\tau} = M J_a^\dagger \ddot{\boldsymbol{x}} + \boldsymbol{\tau}_a, \quad (19)$$

where

$$\boldsymbol{\tau}_a = (C - M J_a^\dagger \dot{J}_a) \dot{\boldsymbol{\theta}} + N - J_a^\top \boldsymbol{\rho}_a. \quad (20)$$

Since the wrench $\boldsymbol{\rho}_a$ is read from the F/T sensor as $(\boldsymbol{f}_S^\top, \boldsymbol{\tau}_S^\top)^\top$, $\boldsymbol{\tau}_a$ will be compensated in control.

A. Pressing

During pressing, the wrench $\boldsymbol{\rho}_a$ exerted at the arm's open end \boldsymbol{a} , is due to the knife-material interaction only, thus $\boldsymbol{\rho}_a = \boldsymbol{\rho}_K$ given in (12). For a desired cutting path $\boldsymbol{x}_d = (a_{xd}, a_{yd}, \phi_d)^\top$, we propose the following position controller:

$$\boldsymbol{\tau} = M J_a^\dagger \boldsymbol{\lambda} + \boldsymbol{\tau}_a, \quad (21)$$

where, letting $\boldsymbol{x}_e = \boldsymbol{x}_d - \boldsymbol{x} = (a_{xe}, a_{ye}, \phi_e)^\top$,

$$\boldsymbol{\lambda} = \begin{pmatrix} \lambda_x \\ \lambda_y \\ \lambda_\phi \end{pmatrix} = \ddot{\boldsymbol{x}}_d + K_{v|a} \dot{\boldsymbol{x}}_e + K_{p|a} \boldsymbol{x}_e + K_{i|a} \int \boldsymbol{x}_e dt. \quad (22)$$

Here, $K_{p|a} = k_{p|a} I_3$, $K_{i|a} = k_{i|a} I_3$, and $K_{v|a} = k_{v|a} I_3$, where I_3 is the 3×3 identity matrix and $k_{p|a}, k_{i|a}, k_{v|a} > 0$, respectively represent proportional, integral, and derivative (PID) gains.

⁴If a real robotic arm has DOFs out of the cutting plane, the dynamics equation should be recalculated by fixing the corresponding joints.

⁵The matrix J_a^\dagger can be replaced by a damped least-square inverse [69]. Note that when $n > 3$, on the right hand side of (17) we could add a term $(I - J_a^\dagger J_a) \boldsymbol{\zeta}$ in the null space of J_a , where $\boldsymbol{\zeta}$ is set to carry out some lower-level objective such as no violation of the joint angle or torque limits, singularity avoidance, or energy minimization [70], [71]. Limit violations and singularity are of little concern in this paper since arm movements during a cutting action are typically within a small range. Task space augmentation is another approach for robot null space control which imposes additionally constrained tasks to be executed alongside the original task with lower priorities [72].

Subtracting the dynamics (19) from the controller (21) and left multiplying the resulting equation by $J_a M^{-1}$, we obtain the following error dynamics:

$$\ddot{\boldsymbol{x}}_e + K_{v|a} \dot{\boldsymbol{x}}_e + K_{p|a} \boldsymbol{x}_e + K_{i|a} \int \boldsymbol{x}_e dt = \mathbf{0}. \quad (23)$$

This is a third order linear time invariant (LTI) system, whose stability can be guaranteed by any $k_{v|a}$, $k_{p|a}$, and $k_{i|a} > 0$ and $k_{v|a} k_{p|a} > k_{i|a}$ [73, pp. 394].

Since a fast knife movement better demonstrates the cutting skill, $\dot{\boldsymbol{x}}_d$ especially its component \dot{a}_{yd} should not be set with a small magnitude. The pressing phase ends when contact between the knife and the cutting board is detected from a sudden increase in the force reading of the F/T sensor. Such increase is due to a knife-board impact.

B. Touching

Upon establishing their contact at a point \boldsymbol{c} (see Fig. 5), the cutting board exerts an impulsive force $\boldsymbol{f} = (f_x, f_y)^\top$ on the knife, which is transmitted to the robotic arm. Since an excessive \boldsymbol{f} value could cause some damage to the arm, there is a need to mitigate it as soon as possible. Meanwhile, the desired x -directional position a_{xd} and orientation ϕ_d of the arm frame \mathcal{A} should be kept constant as the actual values barely vary during the brief period (less than 0.1 s). We thus apply impedance control in the y -direction over a_y (equivalently, on the contact point \boldsymbol{c} 's y -coordinate due to the rigid attachment of the knife at \boldsymbol{a}), while position control over a_x and ϕ . The state is still \boldsymbol{x} given in (13), and therefore, adopts its task space dynamics (19). Since the actual velocities $\dot{\boldsymbol{a}}$ and $\dot{\phi}$ are negligible, all the forces (\boldsymbol{f}_C and \boldsymbol{f}_F) and torques ($\boldsymbol{\tau}_C$ and $\boldsymbol{\tau}_F$) due to material fracture and friction can be ignored. The wrench exerted at \boldsymbol{a} is entirely due to \boldsymbol{f} :

$$\boldsymbol{\rho}_a = \begin{pmatrix} \boldsymbol{f} \\ (\boldsymbol{c} - \boldsymbol{a}) \times \boldsymbol{f} \end{pmatrix}. \quad (24)$$

From the sensed force \boldsymbol{f}_S , we extract \boldsymbol{f} , in particular, its y -component f_y . Then apply hybrid impedance/position control as follows:

$$\boldsymbol{\tau} = M J_a^\dagger \begin{pmatrix} \lambda_x \\ \bar{\lambda}_y \\ \lambda_\phi \end{pmatrix} + \boldsymbol{\tau}_a, \quad (25)$$

where the servos λ_x and λ_ϕ are as in (22), now with zero desired velocity and acceleration, while the servo in the y -direction is

$$\bar{\lambda}_y = \ddot{a}_{yd} + \frac{k_r a_{ye} + d_r \dot{a}_{ye} + f_y}{b_r}, \quad (26)$$

with stiffness k_r , damping d_r , and inertia b_r set for a desired impedance behavior.

Stabilities of a_x and ϕ can be established as described in Section IV-A for the pressing phase. The closed-loop form for a_y is

$$b_r \ddot{a}_{ye} + k_r a_{ye} + d_r \dot{a}_{ye} + f_y = 0.$$

This second order LTI system's stability is ensured by positive gains [73, pp. 394] and bounded f_y [74, pp. 177].

In this phase, impedance control makes the knife-board interaction behave like a mass-spring-damper, which is what

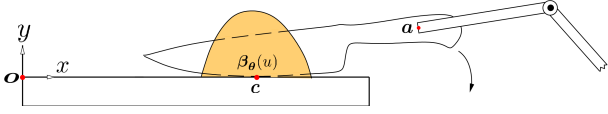


Fig. 6. Slicing along the cutting board.

we need to soften the impact resulting from the fast knife movement in the pressing phase. Force control, on the other hand, would be unable to generate a fast response in this situation.

C. Slicing

Under impedance control, the contact force will experience a significant decrease until it starts to have small fluctuations. The force cannot be precisely regulated due to the applied control policy. In the slicing phase, we apply hybrid control to keep the y -component of this contact force at a certain level to be sure that the object is being split as the knife moves on the cutting board.

The point c of knife-board contact, as illustrated in Fig. 6, has coordinates $(c_x, 0)^T$ if on the cutting board and $\beta_\theta = (\beta_{\theta,x}, \beta_{\theta,y})^T$ if from the knife's edge, as in the world frame \mathcal{W} . Here, we let u be the parameter value of the contact point on the curve β_θ . The two equations

$$\beta_{\theta,x}(u) = c_x, \quad (27)$$

$$\beta_{\theta,y}(u) = 0 \quad (28)$$

hold as long as the contact is maintained. In addition, the tangent at $\beta_\theta(u)$ is parallel to the cutting board, i.e., to the x -axis, yielding

$$\frac{\partial \beta_{\theta,y}}{\partial u} = 0.$$

Applying (6) and $\beta_{\theta,y} = (0, 1)\beta_\theta$, the above equation becomes

$$(\sin \psi, \cos \psi) \frac{d\beta'}{du} = 0. \quad (29)$$

Given the convexity of the knife's edge curve β' , equation (29) defines the location u of the contact point on the edge as a function of the knife's orientation ψ and thus a function of θ according to (4) and (2); that is, $u = u(\theta)$. Constraints (27) and (28) are now rewritten as

$$\beta_\theta(u(\theta)) = \begin{pmatrix} c_x \\ 0 \end{pmatrix}. \quad (30)$$

From the above analysis, the contact point on the knife's edge is determined by c_x and the knife's orientation ψ . The knife is rigid, thus its configuration during slicing can be described by

$$\mathbf{y} = \begin{pmatrix} c_x \\ 0 \\ \psi \end{pmatrix}. \quad (31)$$

The slicing knife is in contact with both the object and the cutting board. The wrench ρ_a at the arm's open end a accordingly has two components:

$$\rho_a = \rho_K + \begin{pmatrix} \mathbf{f} \\ (c - a) \times \mathbf{f} \end{pmatrix}, \quad (32)$$

where ρ_K given in (12) is the wrench due to fracture and friction. The knife-board contact force \mathbf{f} can be estimated by subtracting the calculated force $\mathbf{f}_C + \mathbf{f}_F$ from the sensor reading \mathbf{f}_S of the force component of ρ_a according to (32).

With an objective to maintain the normal contact force f_y , we rewrite the dynamics (16) as

$$\tau = M\ddot{\theta} + C\dot{\theta} + N - J_a^\top \rho_K - J_c^\top \begin{pmatrix} \mathbf{f} \\ 0 \end{pmatrix}, \quad (33)$$

where

$$J_c = \frac{\partial \mathbf{y}}{\partial \theta} = \frac{\partial}{\partial \theta} \begin{pmatrix} \beta_\theta(u) \\ \psi \end{pmatrix} \quad (34)$$

(treating the parameter u as constant so the contact is viewed as a fixed point on the edge) is the $3 \times n$ Jacobian matrix at c .

Our objective is to control c_x and f_y to ensure separation of the object into two pieces when the slicing phase ends. For this purpose we need to further rewrite the dynamics in (33) in terms of \mathbf{y} in the task space. This requires us to make use of the following coordinate transformation:

$$\dot{\mathbf{y}} = L_c \dot{\theta}, \quad (35)$$

where, by (31) and (30),

$$\begin{aligned} L_c &= \frac{\partial}{\partial \theta} \begin{pmatrix} \beta_\theta(u(\theta)) \\ \psi \end{pmatrix} \\ &= J_c + \begin{pmatrix} R(\psi) \frac{\partial}{\partial \theta} (\beta'(u(\theta))) \\ \mathbf{0} \end{pmatrix}. \end{aligned} \quad (36)$$

The second equation above followed from differentiation of equation (6). We have

$$\frac{\partial}{\partial \theta} (\beta'(u(\theta))) = \frac{d\beta'}{du} \nabla u(\theta), \quad (37)$$

where ∇u is a row vector representing the gradient of u . The partial derivatives $\partial u / \partial \theta_i$, for $1 \leq i \leq n$, can be obtained from differentiating the constraint (29) with respect to θ_i . They are all identical, leading to the gradient form:

$$\nabla u = \frac{(-\cos \psi, \sin \psi) \frac{d\beta'}{du}}{(\sin \psi, \cos \psi) \frac{d^2 \beta'}{du^2}} (1, 1, \dots, 1).$$

The dynamics given in (33), via the substitution $\ddot{\theta} = L_c^\dagger (\ddot{\mathbf{y}} - \dot{L}_c \dot{\theta})$ from differentiating (35), become

$$\tau = M L_c^\dagger \ddot{\mathbf{y}} + \tau_c - J_c^\top \begin{pmatrix} \mathbf{f} \\ 0 \end{pmatrix}, \quad (38)$$

where

$$\tau_c = (C - M L_c^\dagger \dot{L}_c) \dot{\theta} + N - J_a^\top \rho_K. \quad (39)$$

Motion planning for the slicing phase is to set a desired time trajectory of c_x and ψ . If the object is easy to cut, a pure translation of the knife (shown in Fig. 7(a)) can be used.

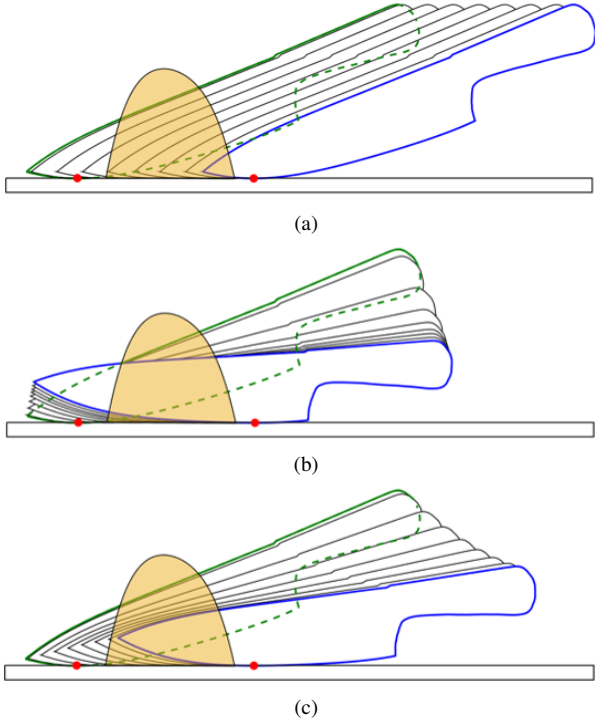


Fig. 7. Three motions for the slicing phase: (a) pure translation, (b) pure rolling, and (c) both translation and rolling.

In this motion, ψ is constant and the contact point does not move on the knife's edge. If the object has a high fracture toughness, a pure rolling motion (shown in Fig. 7(b)) is used so the action becomes "chopping". More commonly, the knife translates and rotates simultaneously, as shown in Fig. 7(c).

Different from in the touching phase, the cutting board is now viewed as rigid enough to prevent penetration by the knife. By choosing a large enough desired normal contact force f_{yd} , we can ensure the actual contact force f_y to be positive despite control errors, namely, the knife to be always in contact with the cutting board. Meanwhile, the x -direction cutting velocity \dot{c}_x and the orientation ψ are under position control. Let $c_{xd}(t)$ be some desired time trajectory of c_x and $c_{xe} = c_{xd} - c_x$ be its error. Let ψ_d be the desired orientation of the knife so $\psi_e = \psi_d - \psi$ is the orientation error. The contact force error is represented by $f_{ye} = f_{yd} - f_y$. We apply the following hybrid control law:

$$\tau = ML_c^\dagger \begin{pmatrix} \ddot{c}_{xd} + k_{v|c}\dot{c}_{xe} + k_{p|c}c_{xe} + k_{i|c} \int c_{xe} dt \\ 0 \\ \ddot{\psi}_d + k_{v|c}\dot{\psi}_e + k_{p|c}\psi_e + k_{i|c} \int \psi_e dt \end{pmatrix} + \tau_c - J_c^\top \begin{pmatrix} f_x \\ f_{yd} + k_{fi} \int f_{ye} dt \\ 0 \end{pmatrix}, \quad (40)$$

where the parameters $k_{p|c}$, $k_{i|c}$, and $k_{v|c}$ are the PID gains, respectively, and k_{fi} is the integral force gain. Although the error dynamics can be easily obtained via a subtraction of (38) from (40), some effort will be involved to separate the

TABLE II
PHYSICAL PARAMETERS IN SIMULATION.

Base of the arm (m)	$\mathbf{b} = (0.6, 0.3)^\top$
Link length (m)	$l_1 = 0.6, l_2 = 0.3, l_3 = 0.3$
Link mass (kg)	$m_1 = 3.5, m_2 = 1.5, m_3 = 1.0$
Link inertia (kg · m ²)	$I_{x1} = 0.0817, I_{x2} = 0.0122, I_{x3} = 0.0081$
Object contour (m)	$y = -8392x^4 + 1606x^3 - 135x^2 + 5x$
Knife tip (m)	$\mathbf{p}'' = (0, -0.2)^\top$
Knife edge (m)	$y' = 74.0x'^4 - 36.15x'^3 + 7.09x'^2 - 0.78x'$
Knife spine (m)	$y' = -37.23x'^4 + 19.7x'^3 - 3.82x'^2 + 0.33x'$

Notes: Base of the arm is in the world frame, while the knife tip position is in the arm frame. The link inertia is taken at the center of mass. The object contour is taken in the world frame and the knife's edge and spine curves are obtained in the knife frame.

TABLE III
GAINS FOR THE CONTROLLERS (21), (25), AND (40) USED IN THE SIMULATION.

Pressing & Touching						Slicing			
$k_{p a}$	$k_{i a}$	$k_{v a}$	k_r	d_r	b_r	$k_{p c}$	$k_{i c}$	$k_{v c}$	k_{fi}
500	800	60	200	100	5	500	800	60	5

part for the positions c_x and ψ from the part for the force f_y , and to establish stabilities for them, respectively. We refer to Appendix B for details.

D. Simulation with a 3-DOF Planar Arm

We use a 3-DOF planar robotic arm, which is the simplest model that can position and orient the knife arbitrarily to realize the cutting scheme described in this section. Widely used robotic arms such as the UR10, 7-DOF WAM, and KUKA LBR iiwa 7 all have at least three revolute joints with parallel axes, and thus can operate like a 3-DOF planar arm.

The three links of the arm assume uniform mass distributions. Table II lists relevant mass, inertia, and geometry information about the arm, object, and knife. Controller gains for simulation are listed in Table III.⁶ The position control gains $k_{p|a}$, $k_{i|a}$, $k_{v|a}$, $k_{p|c}$, $k_{i|c}$, and $k_{v|c}$ are selected to ensure the stability of the LTI system and not generate excessive torques at the arm's joints. The impedance control gain k_r ensures the steady state of the touching phase to have a certain level of contact force⁷, d_r is set to generate a similar amount of counter torque from the velocity as that from the

⁶To predict contact force, a spring model is created for the cutting board with stiffness 5000 N/m to calculate f_y while f_x is set to be 0. Since the cutting board is no longer treated as a rigid environment, a derivative term with gain 0.04 is added to the force control term $f_{yd} + k_{fi} \int f_{ye} dt$ in (40) for the slicing phase.

⁷This phase terminates before reaching the steady state.

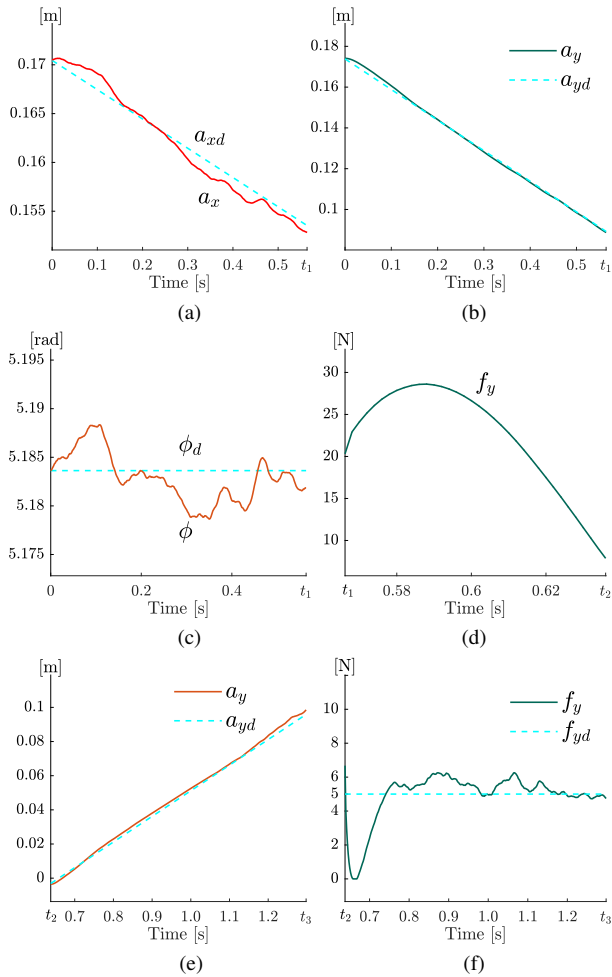


Fig. 8. Simulated cutting action with a 3-DOF planar arm (the three cutting phases: pressing, touching, and slicing start at 0s, $t_1 = 0.564$ s, and $t_2 = 0.636$ s, respectively, and the cutting action ends at $t_3 = 1.30$ s): (a)–(c) desired and actual position and orientation of the arm frame during the pressing phase, (d) knife-board contact force in the touching phase, and (e)–(f) desired and actual knife-board contact position and force in the slicing phase. We use $\dot{a}_{yd} = -0.15$ m/s during pressing and $\dot{c}_{xd} = 0.15$ m/s in slicing as desired values.

contact force at the beginning of the touching phase, and b_r is set to be close to the total mass of all the robot links. The force control gain k_{fi} is set to a low value to avoid oscillations of the contact force. The wrench ρ_K in (12), due to cutting and frictional forces on the knife, is applied in both inverse and forward dynamics, thus gets eliminated and does not need to be calculated. Hence, we do not need fracture toughness, pressure distribution, or coefficient of friction in simulation. All the three phases of cutting, in their forward dynamics, are subjected to force and torque disturbances that are uniformly distributed within the ranges $[-2.5, 2.5]$ N and $[-0.25, 0.25]$ N·m, respectively.

Shown in Fig. 8(a)–(c) are the actual and desired positions and orientations of the arm frame \mathcal{A} during the pressing phase with maximum gaps of 0.002 mm, 0.001 m, and 0.005 rad, respectively. Plot (d) shows that knife-board contact force drops significantly (from 28 N to 8 N) in the ephemeral (0.072 s) touching phase. In (e), the gap between the actual and desired x -directional positions of c is almost negligible. In (f), the y -

component f_y of the knife-board contact force is kept close to the desired value (5 N).

V. DYNAMIC ESTIMATION OF PHYSICAL PARAMETERS

The object's fracture toughness κ varies with the knife's sharpness. Its coefficient μ of friction with the blade depends on the latter's material. The values of both parameters also vary among natural foods, whether or not of the same type, and for the same food, with its degree of freshness and between its skin and interior. Pressure on the object being cut depends on the thickness of the blade. It may vary from point to point inside the region Ω of the blade-material contact, and at the same point, from one time instant to another during the cutting action.

The parameters κ , μ , and the pressure distribution function $P(x, y)$ are only used in the last phase (slicing) for modeling the fracture and frictional forces \mathbf{f}_C and \mathbf{f}_F in order to estimate the knife-board contact force \mathbf{f} from the sensed force $\mathbf{f}_S = \mathbf{f}_C + \mathbf{f}_F + \mathbf{f}$ for control purpose. Since the second phase (touching) is very brief, we can conveniently make use of the force data accumulated during the first phase (pressing) to estimate κ , μ , and $P(x, y)$ for the object, and apply these values in modeling during the last phase (slicing).

Some simplifications are necessary for such real-time estimation. First, it is reasonable for us to treat κ and μ as constants throughout cutting. Next, $P(x, y)$ is approximated as a uniform (but time varying) pressure distribution over the contact region Ω . This simplifies the frictional force (10) to

$$\mathbf{f}_F \approx -2\mu P \iint_{\Omega} \hat{v} \, dx dy. \quad (41)$$

From experimental data, we have found that P decreases during the pressing phase. The decrease may be attributed to release of some stress due to fracture. Let P_{\max} be its maximum value. Let Φ be the area of fracture so far. (Its maximum value Φ_{\max} corresponds to the area of intersection between the object and the cutting plane.) The pressure distribution at the time instant is modeled linearly as

$$P = \frac{\Phi_{\max} - \Phi}{\Phi_{\max}} P_{\max}. \quad (42)$$

Observing in equation (41) that μ and P are multiplied together, we treat μ and P_{\max} as a single term

$$\delta = \mu P_{\max} \quad (43)$$

to be determined.

The F/T sensor mounted at the robotic arm's open end acquires its readings at equally spaced time instants. During the pressing phase, since the knife is in contact with the object only, the sensed force is $\mathbf{f}_S = \mathbf{f}_C + \mathbf{f}_F$. The first reading used for estimation is obtained after the knife has cut into the object for some distance and the y -directional velocity has reached a desired constant value. The last reading is obtained when the lowest point on the knife edge is several millimeters above the cutting board. The time instant of the first reading is indexed 1 and that of the last reading used for estimation is indexed n_S .

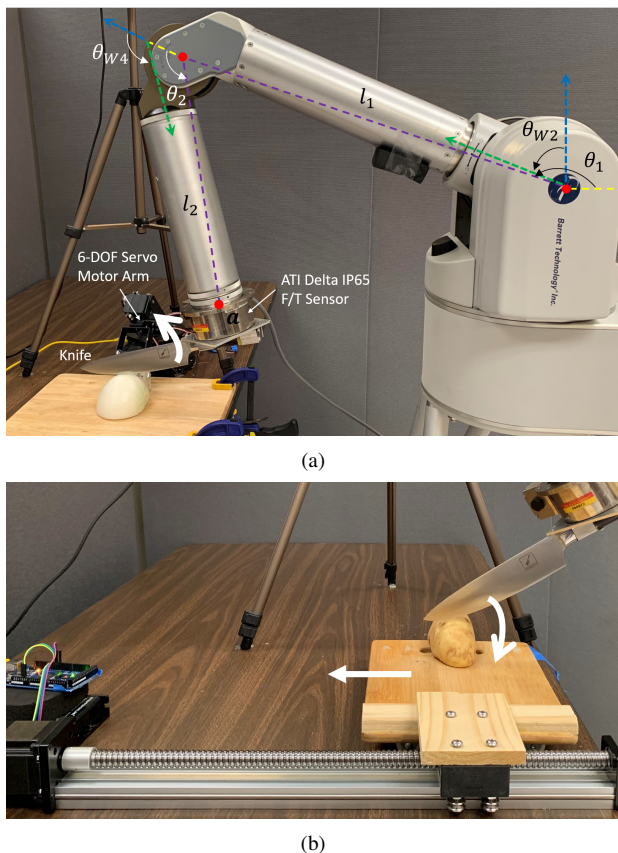


Fig. 9. Experimental setups. Joints 2 and 4 of a WAM arm, with angles θ_{W2} and θ_{W4} , respectively, are mapped to the joints of the 2-link arm in Fig. 2 with $\theta_1 = \theta_{W2} + 1.652433$ and $\theta_2 = \theta_{W4} - 0.209506$. The equivalent lengths of the two links are $l_1 = 0.551838$ m and $l_2 = 0.352881$ m. Two setups (a) and (b) allow for counterclockwise and clockwise knife rotations (indicated by curved white arrows) during the slicing phase, respectively. In (b), an extra DOF is provided by a linear guide (bottom), which translates the cutting board leftward to help realize a knife motion close to rolling so a “chop” can be performed.

We estimate κ and δ via minimizing the sum of the squared difference between the sensed force $\mathbf{f}_{S,j}$ and its modeled value $\mathbf{f}_{C,j} + \mathbf{f}_{F,j}$ over all the time instants j , $1 \leq j \leq n_S$. Let us rewrite $\mathbf{f}_C = \kappa \chi_C$ and $\mathbf{f}_F = \delta \chi_F$, where χ_C is extracted from (8) after substituting in (7) and χ_F is extracted from (41) after substituting in (42) and then applying (43). Then, κ and δ can be estimated via least-squares fitting:

$$\min_{\kappa, \delta} \sum_{j=1}^{n_S} (\mathbf{f}_{S,j} - \kappa \chi_{C,j} - \delta \chi_{F,j})^2. \quad (44)$$

Closed forms for the optimal values of κ and δ can be easily obtained from vanishing of the gradient of the cost function in (44).⁸

VI. EXPERIMENTS

Cutting experiments were carried out with a 4-DOF WAM Arm shown in Fig. 9(a). Its joints 1 and 3 were out of the

⁸Occasionally, δ may end up with a negative optimal value. When this happens, we apply Newton’s method [75, pp. 484–487] with initial values such as $\kappa = 300$ N/m and $\delta = 2000$ N/m². The method iterations will terminate when δ gets close to 0.

cutting plane and thus fixed, so the robot effectively had two DOFs. Mounted on the arm’s end effector was a 6-axis Delta IP65 F/T sensor from ATI Industrial Automation. Rigidly attached to the F/T sensor through a metal adaptor was a kitchen knife, whose kinematics were in terms of the robot’s joint angles. To apply the dynamics equation (16), we calculated the combined mass, Coriolis, and gravity terms (M , C , and N , respectively) of the arm, sensor, adaptor, and knife based on the specifications of the arm [76] and the sensor.

To model the kitchen knife, we placed it on a sheet of paper, and drew its contour. After choosing the x' - and y' -axes of the knife frame \mathcal{K} at the knife point, we reconstructed the knife’s edge curve $\beta'(u)$ by setting u to be the x' -coordinate and fitting a quartic curve β'_y to the y' -coordinates of the measured points on the edge. Similarly, the knife’s spine curve was reconstructed through fitting as a quartic curve $\gamma'(q) = (q, \gamma'_y(q))^T$ with q identified with x' .

A Microsoft Kinect sensor supported by a tripod acquired some densely distributed points on the object’s surface. Those points close enough to the cutting plane were fit over to reconstruct the contour $\sigma(r)$ of the object’s cross section in the cutting plane. A 6-DOF Servo Motor Arm held the object to stabilize it during cutting.

For the three phases of cutting, we reused all the controller gains in Table III except those of $k_{v|a}$, b_r , and $k_{v|c}$. Smaller differential gains $k_{v|a} = 35$ and $k_{v|c} = 35$ were used to avoid oscillations due to minor fluctuations in the WAM arm’s velocity. The gain $b_r = 10$ was adopted for being closer to the combined mass of the links, the ATI sensor, and the knife. Note that the same PID gains were used for the x -directional position control throughout the three phases to ensure the continuity of the commanded torque. Since different control policies were applied in the y -direction during the three phases, the commanded joint torque always went through a smoothing filter before being sent to the arm.

Onions, potatoes, apples, and cucumbers were used in the experiments. In a cutting trial, half of an object (precut by the human hand) was placed on the cutting board with its flat face down (see the onion and potato in Fig. 9(a) and (b), respectively).

A. Cutting with a 2-DOF Planar Robotic Arm

The three-phase cutting strategy presented in Section IV is for a planar arm with three or more DOFs. The strategy first needs to be adapted to the WAM Arm due to its two DOFs in the cutting plane. This affects the control policies for all three phases of cutting.

In the pressing phase, the position of the arm’s open end is simplified from (1) given $n = 2$:

$$\mathbf{a} = \begin{pmatrix} a_x \\ a_y \end{pmatrix} = l_1 \begin{pmatrix} \cos \theta_1 \\ \sin \theta_1 \end{pmatrix} + l_2 \begin{pmatrix} \cos \phi \\ \sin \phi \end{pmatrix}, \quad (45)$$

where $\phi = \theta_1 + \theta_2$. We keep a constant orientation ψ defined in (4) of the knife, whose state is then given by \mathbf{a} alone. The trajectory of \mathbf{a} must be a circle centered at $(l_2 \cos \phi, l_2 \sin \phi)^T$ and with radius l_1 . The knife’s initial orientation thus uniquely determines the desired trajectory $\mathbf{a}_d = (a_{xd}, a_{yd})^T$.

The arm's open end has the velocity $\dot{\mathbf{a}} = \bar{J}_a \dot{\boldsymbol{\theta}}$, where the 2×2 Jacobian matrix $\bar{J}_a = \partial \mathbf{a} / \partial \boldsymbol{\theta}$ includes only the first two rows of J_a in (15). We differentiate $\dot{\mathbf{a}}$ and substitute the resulting equation for $\dot{\boldsymbol{\theta}}$ into (16). This yields the following dynamic equation which is similar to (19):

$$\boldsymbol{\tau} = M \bar{J}_a^{-1} \ddot{\mathbf{a}} + \bar{\boldsymbol{\tau}}_a, \quad (46)$$

where

$$\bar{\boldsymbol{\tau}}_a = (C - M \bar{J}_a^{-1} \dot{\bar{J}}_a) \dot{\boldsymbol{\theta}} + N - J_a^\top \boldsymbol{\rho}_a.$$

The controller to be applied replaces $\ddot{\mathbf{a}}$ in (46) with a PID servo in terms of a desired acceleration $\ddot{\mathbf{a}}_d$ and the error $\mathbf{a}_e = \mathbf{a}_d - \mathbf{a}$.

The touching phase, described in Section IV-B, aims to soften the contact between the knife and cutting board. With the same state \mathbf{a} , the task space dynamics equation (46) still holds. The hybrid position and impedance controller (25) is simply adapted for the 2-DOF arm:

$$\boldsymbol{\tau} = M \bar{J}_a^{-1} \begin{pmatrix} \lambda_x \\ \lambda_y \end{pmatrix} + \bar{\boldsymbol{\tau}}_a. \quad (47)$$

In the slicing phase, the contact constraints (27)–(29) along with (4) uniquely determine θ_1 , θ_2 , and u as functions of c_x , hence the path of the knife. We write $\boldsymbol{\theta} = \boldsymbol{\theta}(c_x)$ and $u = u(c_x)$. The knife is unable to roll on the cutting board to execute chopping. This is reasoned below. Rolling would require the x -velocity of the instantaneous contact point on the knife's edge to be zero, equivalently, $(1, 0) \bar{J}_c(\boldsymbol{\theta}) \dot{\boldsymbol{\theta}} = 0$, where $\bar{J}_c = \partial \boldsymbol{\beta}_\theta / \partial \boldsymbol{\theta}$ includes only the first two rows of J_c given in (34). With $\dot{\boldsymbol{\theta}} = (d\boldsymbol{\theta}/dc_x) \dot{c}_x$ substituted in, the above condition becomes $(1, 0) \bar{J}_c(\boldsymbol{\theta}) (d\boldsymbol{\theta}/dc_x) \dot{c}_x = 0$. To make steady progress toward cutting open the object, either $\dot{c}_x > 0$ throughout cutting or $\dot{c}_x < 0$ throughout cutting must hold. Hence, rolling would require

$$(1, 0) \bar{J}_c(\boldsymbol{\theta}) \frac{d\boldsymbol{\theta}}{dc_x} = 0. \quad (48)$$

Equation (48) is independent from equations (27)–(29) derived from the contact geometry. Together the four equations cannot be simultaneously satisfied by the three variables θ_1 , θ_2 , and u . The knife's motion during slicing, driven by the 2-DOF arm, is neither pure translation nor pure rolling, with the contact point moving less on the knife's edge than on the cutting board.

The state is now $\bar{\mathbf{y}} = (c_x, 0)^\top$. Denote by \bar{L}_c the 2×2 matrix made up of the first two rows of L_c given in (36). The task space dynamics equation (38) now takes the form

$$\boldsymbol{\tau} = M \bar{L}_c^{-1} \ddot{\bar{\mathbf{y}}} + \bar{\boldsymbol{\tau}}_c - J_c^\top \begin{pmatrix} \mathbf{f} \\ 0 \end{pmatrix},$$

where

$$\bar{\boldsymbol{\tau}}_c = (C - M \bar{L}_c^{-1} \dot{\bar{L}}_c) \dot{\bar{\mathbf{y}}} + N - J_a^\top \boldsymbol{\rho}_K.$$

A hybrid position/force controller is then adapted from (40):

$$\boldsymbol{\tau} = M \bar{L}_c^{-1} \begin{pmatrix} \ddot{c}_{xd} + k_v |c_{xe} + k_p |c_{xe} + k_i |c \int c_{xe} dt \\ 0 \end{pmatrix} + \bar{\boldsymbol{\tau}}_c - J_c^\top \begin{pmatrix} f_x \\ f_{yd} + k_{fi} \int f_{ye} dt \end{pmatrix}. \quad (49)$$

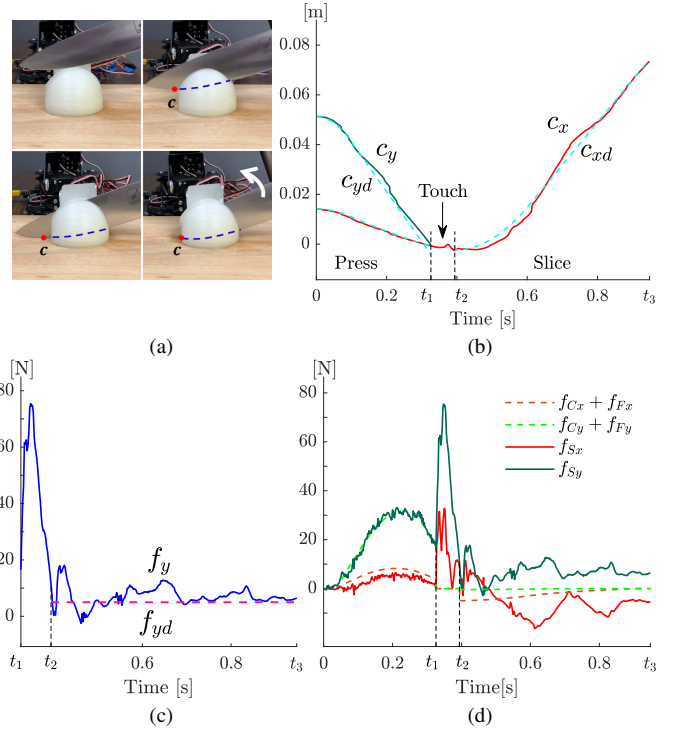


Fig. 10. Cutting of an onion with the setup in Fig. 9(a). (a) Snapshots at the start and during the three phases: pressing, touching, and slicing. The cutting action ended at $t_3 = 0.948$ s. The dashed lines draw out the occluded portions of the knife's edge, c marks the lowest point on the knife's edge, and the white arrow in the last snapshot shows the knife's counterclockwise rotation during the slicing phase. We used $\dot{a}_{yd} = -0.2$ m/s and $\dot{c}_{xd} = 0.17$ m/s as the desired values for pressing and slicing, respectively. Trajectories of (b) the lowest point c on the knife's edge, (c) the y -component f_y of the contact force between the knife and cutting board and its desired value $f_{yd} = 5$ N, and (d) the sensor reading $\mathbf{f}_S = (f_{Sx}, f_{Sy})^\top$ (drawn in solid lines) of the force exerted on the knife, and the sum $\mathbf{f}_C + \mathbf{f}_F = (f_{Cx} + f_{Fx}, f_{Cy} + f_{Fy})^\top$ (drawn in dashed lines) of modeled fracture and frictional forces. The parameter values estimated at the end of pressing and then used in slicing were $\kappa = 302.13$ N/m and $\delta = 15961.8$ N/m².

B. Control Validations for Pressing and Touching

Fig. 10(a)–(d) shows the experimental results from cutting an onion. Pressing, touching, and slicing lasted over the time periods $[0, t_1)$, $[t_1, t_2)$, and $[t_2, t_3]$, respectively. The pressing phase, during which the knife was translating, started with the knife slightly above the object and ended when the knife-board impact was detected from sensor readings. The touching phase softened this impact within a short time period before it smoothly transitioned into the slicing phase.

Included in Fig. 10(a) are four snapshots respectively at the start and during the three phases, which started at 0 s, $t_1 = 0.326$ s, and $t_2 = 0.394$ s, respectively. With a slight abuse of notation we let $c = (c_x, c_y)^\top$ also denote the lowest point on the knife's edge during the pressing phase (when the knife is not in contact with the board). In (b), the ordinate c_y follows the desired trajectory c_{yd} over $[0, t_1)$ and the abscissa c_x follows the desired trajectory c_{xd} over $[0, t_3]$. Since the knife was rigidly connected to the robot and its orientation was kept constant during the pressing period $[0, t_1)$, the actual and desired trajectories of c were simply translated from those of \mathbf{a} . Fig. 10(c), plotted over the period $[t_1, t_3]$, shows that the contact force decreased from 75 N to 11 N within 0.068 s

under impedance control during touching, and then approached the desired value with small variations under force control. As seen in (d), in the pressing phase the modeled frictional force f_F (between the blade and the material) and fracture force f_C , even though not used, add up close to the sensed force f_S . This provides assurance for their modeled values to be used in the slicing phase.

As observed from Fig. 10(d), during slicing the sum $f_{C_y} + f_{F_y}$ of the y -directional fracture and frictional forces was almost negligible. This was in fact caused by the WAM Arm's lack of one DOF to achieve an arbitrary pose of the knife in the cutting plane. Here is an explanation. To maintain the knife-board contact (i.e., $c_y = 0$) equivalently took away one of the two DOFs of the arm in the cutting plane. During slicing, the remaining DOF carried out a path of knife poses which was completely determined. (How fast the knife moved along the path could still be realized via controlling the change rate of this second DOF.) Meanwhile, to cut through the object, this path was also subjected to the constraint that the knife-board contact point c had to move across the bottom segment of the object's cross section in the cutting plane, say, from left to right. As c was moving in this direction, the knife was rotating counterclockwise while the contact point was moving on its edge towards the tip. This required c to be located several centimeters away from the tip at the start of slicing, resulting in the knife just slightly tilted. The knife consequently was having a very small vertical velocity component relative to its horizontal one. Under the knife's counterclockwise rotation, only those points on its edge to the right of the contact point were generating fracture. The rotation also resulted in partial canceling of the y -components of the frictional forces exerted on points within the knife-blade contact region Ω . This was why $f_{C_y} + f_{F_y}$ turned out to be negligible in Fig. 10(d).⁹

C. Control Validation for Slicing

To generate a large downward cutting force f_{C_y} , the knife needed to perform an action close to "rock chop", by starting the third phase in a more tilted pose and rotating clockwise so its edge would be ideally rolling on the cutting board. This was impossible with the arm's two DOFs in the cutting plane. We switched to the second setup in Fig. 9(b), where a linear guide was used to translate the board leftward.

The world frame \mathcal{W} was fixed and not moving with the board. The contact motion $c_x(t)$ was relative to the still x -axis not the translating board. As discussed in Section VI-A, $\theta = \theta(c_x)$ for a 2-DOF arm. Rolling of the knife on the board would be achieved by setting the board's x -velocity v to be equal to that of the instantaneous contact point on the knife's edge:

$$v = v_c \equiv (1, 0) \bar{J}_c(\theta(c_x)) \frac{d\theta}{dc_x}(c_x) \dot{c}_x, \quad (50)$$

where $\bar{J}_c = \partial \beta_\theta / \partial \theta$ was introduced in Section VI-A. However, the obtained v , constantly changing with time, could not be generated accurately enough by the linear guide. Instead, we kept v at some constant value (-0.04 m/s) and constructed

⁹There would have been no change to the situation had the knife been moving along the path in the opposite direction.

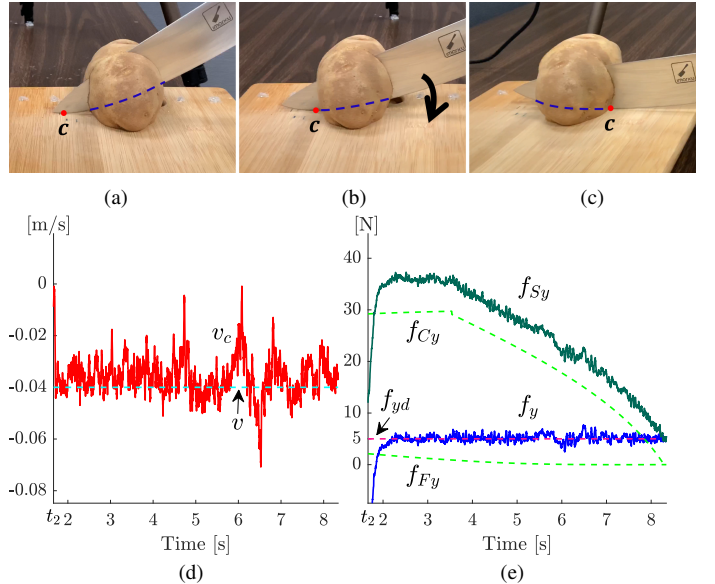


Fig. 11. Slicing phase of cutting a potato with the setup in Fig. 9(b). Snapshots of slicing: (a) start, (b) middle, and (c) end. (d) Velocity v of the cutting board vs. velocity v_c of the instantaneous contact point on the knife's edge ($t_2 = 1.612$ s). (e) The y -components f_{C_y} and f_{F_y} of the modeled fracture and frictional forces, respectively, the desired normal contact force $f_{y,d}$, and its estimate $f_y = f_{S_y} - f_{C_y} - f_{F_y}$. Fitting at the end of the pressing phase estimated $\kappa = 463.76$ N/m and $\delta = 2565.23$ N/m².

a desired contact motion $c_{xd}(t)$ to satisfy equation (50) approximately. More specifically, we evaluated the derivative:

$$\dot{c}_{xd} = \frac{v}{(1, 0) \bar{J}_c(\theta(c_{xd}))} \frac{d\theta}{dc_x}(c_{xd}) \quad (51)$$

at the time instant, integrated over a time step to update c_{xd} at the next time instant, and so on.

Fig. 11 focuses on the slicing phase of cutting a potato in the setup of Fig. 9(b) using the $c_{xd}(t)$ constructed from (51), with three snapshots shown in (a)–(c). The near-rolling motion of the knife is evidenced in (d) from a small range of difference between the time trajectories of v and v_c in (50). The fluctuations of v_c were in a degree caused by the uneven cutting board which was made of bamboo. As shown in Fig. 11(e), the modeled y -directional fracture force f_{C_y} was almost 30 N at the beginning of slicing. It first increased slightly as c was moving into the object and then gradually decreased to 0 when the object was cut open. The contact force component f_y was maintained close to the desired value of 5.0 N. The modeled frictional force, with its y -component f_{F_y} at 2.0 N when the slicing phase started, kept decreasing as the pressure distribution decreased.

D. Comparison with Cutting under Position Commands

We tested alternative approaches for comparisons with our proposed controllers. The first such alternative was to execute joint position commands (JPC) on the WAM arm, whose built-in controller then took these commands as input. The joint positions were obtained from our planned Cartesian space trajectories through inverse kinematics. Not surprisingly, the JPC approach worked well in the pressing phase.

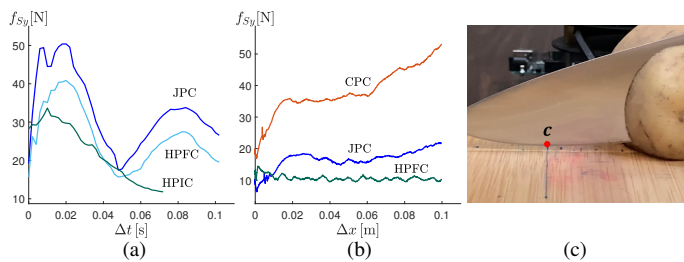


Fig. 12. Cutting with alternative approaches. (a) Time trajectories of the sensed y -directional force f_{Sy} during the touching phase respectively under joint position commands (JPC), the hybrid position/force controller (HPFC) given in (49), and the hybrid position/impedance controller (HPIC) given in (47). (b) Trajectories of the sensed y -directional force f_{Sy} during the slicing phase respectively under the JPC, the Cartesian space position controller (CPC) given in (52), and the HPFC given in (49) with the setup in Fig. 9(a). (c) Snapshot from the slicing phase of cutting a potato under the JPC with the setup in Fig. 9(b). The lowest point c on the knife's edge is above the board in this snapshot, implying a contact break.

In the touching phase, we tried separately the JPC to maintain constant joint angles and the hybrid position/force controller (HPFC) given in (49) to maintain constant x -directional position and y -directional force. As shown in Fig. 12(a), both approaches resulted in the y -directional force readings by the F/T sensor increasing again after dropping to a lower level and caused the transitional touching phase still not to terminate after 0.1s. In contrast, under the hybrid position/impedance controller (HPIC) given in (47), the force readings decreased until below a preset level to end the touching phase after 0.07s.

In the slicing phase, we tested the JPC and a Cartesian position controller (CPC) modified from (49) as follows:

$$\begin{aligned} \boldsymbol{\tau} = M\bar{L}_c^{-1} & \begin{pmatrix} \ddot{c}_{xe} + k_{v|c}\dot{c}_{xe} + k_{p|c}c_{xe} + k_{i|c} \int c_{xe} dt \\ k_{v|c}\dot{c}_{ye} + k_{p|c}c_{ye} + k_{i|c} \int c_{ye} dt \end{pmatrix} \\ & + (C - M\bar{L}_c^{-1}\dot{\bar{L}}_c)\dot{\boldsymbol{\theta}} + N - J_a^T \begin{pmatrix} \mathbf{f}_S \\ \boldsymbol{\tau}_S \end{pmatrix}. \end{aligned} \quad (52)$$

Both policies were able to maintain a constant y -position, either on the board surface for the setup in Fig. 9(a) or slightly below the surface for that in Fig. 9(b). Fig. 12(b) compares the force trajectories resulting from these two approaches to that from the HPFC given in (49). The knife-board contact force kept increasing under the JPC and CPC, but stayed around 10N under the HPFC. It was evident that the JPC and CPC, especially the later, applied excessive forces on the cutting board. For the setup in Fig. 9(b), neither the JPC nor the CPC was able to maintain the knife-board contact during the slicing phase. The snapshot in Fig. 12(c) from cutting a potato shows that the knife had broken its contact with the cutting board under the JPC (the same situation also happened under the CPC). The potato was not fully cut open as a result.

To summarize, position control can neither handle the knife-board impact in the touching phase nor maintain the knife board contact force in the slicing phase of the cutting action. There are several reasons. First, high accuracy of the knife's position is not easy to achieve, considering both its not so rigid connection to the moving robotic arm and its estimated edge curve for calculation of the contact point. Second, in order to

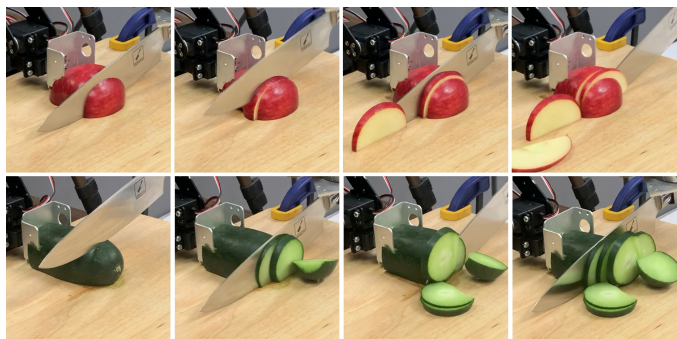


Fig. 13. Repeated cutting of an apple and a cucumber with the setup in Fig. 9(a).

avoid a large impact with the cutting board, the velocity of cutting would have to be slow under position control, which is not desired for swiftness of cutting. It is more effective to mitigate the impulsive force for smoothness and swiftness and to prevent any damage to the arm. Third, breaking of the knife-board contact can happen to result in the object not being cut through. Finally, the contact force between the knife and the cutting board can change dramatically with a tiny position error (especially when the board has a hard surface), which would be unavoidable and potentially harmful to the robotic arm. The survey [77] gives detailed explanations of why force control is preferred in tasks where a robot manipulates an object or performs operations on a surface.

E. Repeated Cutting

We conducted more experiments with the three-phase cutting strategy. After each cutting action, the small 6-DOF Servo Motor Arm (see Fig. 9(a)) pushed the uncut portion of the object forward for a small distance on the cutting board. This made it possible to cut the object into pieces by repeating the same three-phase knife movement. Fig. 13 includes some snapshots from cutting an apple and a cucumber into pieces.

VII. SUMMARY

This paper is about how to enable a robotic arm to perform a natural and smooth cutting action. Complexity arises due to the heavy presence of contacts encountered by the knife (with the object and cutting board). We have sequenced the entire action into three phases (pressing, touching, and slicing), drawing an inspiration from kitchen knife maneuvers by the human hand. Employed in each phase are one or multiple control policies to accommodate its specific subgoal and contact constraints.

A. Discussion

There are several advantages of using the introduced three-phase cutting scheme. First, the action looks natural and resembles the human's cutting action, thanks to smooth transitions of controllers among the three phases. Second, fast cutting is realized. In our experiments (with the setup in Fig. 9(a)), a fruit or vegetable was cut open within 0.1 s. Third, complete material separation is achieved because estimation of the knife-board contact force ensures the object to be cut

through under hybrid control in the slicing phase. Finally, controls based on regulating the knife-board contact force during the touching and slicing phases effectively protect the robotic arm by avoiding excessive contact forces from the cutting board.

Estimation of the knife-board contact force is made possible by modeling based on fracture mechanics. This allows us to separate, from the F/T sensor reading, forces of different sources such as fracture, knife-material contact, and knife-board contact. Under a cutting action such as rock chop (see Fig. 11(e)), the fracture force is significantly larger than the needed knife-board contact force, which makes force modeling indispensable to maintain the contact and meanwhile avoid an excessive amount of force applied there. The authors' recent work [78] showed that it is possible to use force sensing and modeling to track the changes in the material properties such as the Poisson's ratio, fracture toughness, and coefficient of friction. Such information can be used for dynamically adjusting the knife's moving direction to reduce effort.

The three-phase cutting scheme can be easily transferred to a different robotic arm based on its own model of dynamics. The control policies would be easily adapted for cutting deformable objects, as long as the fracture and frictional forces and the status of deformation can be estimated in real time.

In fact, computation for the presented controllers can be immediately reduced, albeit in a limited way. In the experiments, we noticed that, since cutting was carried out in a small operational space, the WAM Arm's inertial matrix M did not vary much during the action. In fact, additional experiments, conducted with constant M values chosen at the middle of the three phases and the $\dot{\theta}$ terms removed from (19) and (38) for τ_a and τ_c , respectively, claimed similar outcomes as those from using the arm's accurate dynamic model.

B. Future Work

An immediate extension of this work will be to an object undergoing small deformations from cutting. The fracture and contact forces (frictional forces included), along with the areas of fracture and contact and the object's deformation, can be modeled using the FEM. This can be done through "solving" an equation that describes a balance between the work conducted by the knife and the total amount spent on creation of fracture, dissipated through friction, and converted into or from strain energy.¹⁰ An obstacle will be the high computational cost with an additional level of discretization (of the knife's motion) needed to model the continuous phenomenon.

For planning of and real-time adjustments to a cutting trajectory, it is quite important to efficiently generate reliable force and shape predictions along hypothesized trajectories. We hope to compensate modeling inaccuracies with force sensing, vision, and improved knife control. In the longer term, we would like to investigate cutting of objects with large deformations and viscosities, for which modeling of strain energy and viscous force will be essential.

¹⁰Some preliminary work [79] was carried out in the lab directed by the third author.

Smoothness of cutting by the human hand comes from its speed and energy efficiency. We would like to investigate cutting paths that minimize cost functions such as work done by the knife or arm, fracture toughness along the path, degree of deformation, etc. Energy based real-time optimal cutting for a translating knife has been proposed in [78]. More efforts are needed on planning an optimal path for a knife under rotation.¹¹ Path optimization could also make use of null space control in case the arm has more than three DOFs in the cutting plane, by using a weighted pseudoinverse in terms of acceleration [71], [82].

A fourth direction of extension is to have the kitchen knife, instead of rigidly attached to the arm, held by a robotic hand driven by the arm. The system will become more autonomous since the hand can put down the knife, attend to another task, and pick up the knife again. There will be more dexterity because control of the knife is directly done by the hand. A humanoid robot would directly benefit from the development to grasp a kitchen knife for food preparation in the kitchen. There are challenges to face. Cutting control will have to consider higher degrees of freedom, compliance of contact between the knife's handle and the hand, and (possibly) finger gaits for adjusting a grasp on the knife. Involvement of a second robotic arm (with a mounted hand) to stabilize and maneuver the object being cut will bring up the issues of arm-arm and arm-hand coordinations.

At a higher level, we will look at implementation of different knife skills including chop, slice, dice, roll cut, etc. Knife paths obtained through optimization will be expected to become new knife skills suitable to the robotic arm.

APPENDIX A

COMPUTATION OF FRACTURE AND FRICTIONAL FORCES FOR A TRANSLATING KNIFE

When the knife keeps a constant orientation, all the points on its blade are moving at the same velocity \mathbf{v} . Denote $\hat{\mathbf{v}} = \mathbf{v}/\|\mathbf{v}\| = (\hat{v}_x, \hat{v}_y)^\top$. Calculation of fracture and frictional forces and torques can be simplified. The integral (8) for the fracture force now has a closed form:

$$\begin{aligned} \mathbf{f}_C &= \int_{u_1}^{u_2} \kappa \hat{\mathbf{v}} \cdot \left(-\frac{d\beta_{\theta,y}}{du}, \frac{d\beta_{\theta,x}}{du} \right)^\top \hat{\mathbf{v}} du \\ &= \kappa \left(\hat{\mathbf{v}} \cdot \left(-\beta_{\theta,y}, \beta_{\theta,x} \right) \Big|_{u_1}^{u_2} \right) \hat{\mathbf{v}}. \end{aligned} \quad (53)$$

The integral (9) for the torque due to fracture can be simplified:

¹¹Energy-saving trajectory planning for manipulators has been considered in works such as [80], [81].

$$\begin{aligned}
\tau_C &= \int_{u_1}^{u_2} \left(\boldsymbol{\beta}_\theta(u) - \mathbf{a} \right) \times \kappa \left(\hat{\mathbf{v}} \cdot \left(-\frac{d\beta_{\theta,y}}{du}, \frac{d\beta_{\theta,x}}{du} \right)^\top \hat{\mathbf{v}} \right) du \\
&= \kappa \hat{\mathbf{v}} \cdot \int_{u_1}^{u_2} \left((\boldsymbol{\beta}_\theta(u) - \mathbf{a}) \times \hat{\mathbf{v}} \right) \left(-\frac{d\beta_{\theta,y}}{du}, \frac{d\beta_{\theta,x}}{du} \right)^\top du \\
&= \kappa \hat{\mathbf{v}} \cdot \left(- \left(\begin{array}{c} -\beta_y \\ \beta_x \end{array} \right) \Big|_{u_1}^{u_2} (\mathbf{a} \times \hat{\mathbf{v}}) + \frac{1}{2} \left(\begin{array}{c} \beta_{\theta,y}^2 \hat{v}_x \\ \beta_{\theta,x}^2 \hat{v}_y \end{array} \right) \Big|_{u_1}^{u_2} \right. \\
&\quad \left. - \int_{u_1}^{u_2} \left(\begin{array}{c} \beta_{\theta,x} \beta'_{\theta,y} \hat{v}_y \\ \beta'_{\theta,x} \beta_{\theta,y} \hat{v}_x \end{array} \right) du \right). \quad (54)
\end{aligned}$$

Under Green's theorem, the area A of the knife-material contact can be calculated along its boundary $\partial\Omega$ as follows:

$$\begin{aligned}
A &= \iint_{\Omega} dx dy = \oint_{\partial\Omega} x dy \\
&= \int_{u_1}^{u_2} \beta_{\theta,x} d\beta_{\theta,y} + \int_{r_2}^{r_3} \sigma_x d\sigma_y + \int_{q_2}^{q_1} \gamma_{\theta,x} d\gamma_{\theta,y} \quad (55) \\
&\quad + \int_{r_4}^{r_1} \sigma_x d\sigma_y.
\end{aligned}$$

When the pressure distribution P is uniform, the frictional force (10) and its generated torque (11) are

$$\begin{aligned}
\mathbf{f}_F &= -2\mu P A \hat{\mathbf{v}}, \quad (56) \\
\tau_F &= -2\mu P \iint_{\Omega} \left(\begin{array}{c} x \\ y \end{array} \right) - \mathbf{a} \times \hat{\mathbf{v}} dx dy \\
&= 2\mu P A \mathbf{a} \times \hat{\mathbf{v}} - 2\mu P \iint_{\Omega} \left(\begin{array}{c} x \\ y \end{array} \right) \times \hat{\mathbf{v}} dx dy \\
&= 2\mu P A \mathbf{a} \times \hat{\mathbf{v}} - 2\mu P \iint_{\Omega} (xv_y - yv_x) dx dy \\
&= 2\mu P A \mathbf{a} \times \hat{\mathbf{v}} - 2\mu P \int_{\partial\Omega} \left(\frac{x^2}{2} v_y - xyv_x \right) dy. \quad (57)
\end{aligned}$$

The integrals (53)–(57) have closed forms when the curves β_θ and γ_θ of the knife's edge and spine and σ bounding the object's cross section are parameterized using polynomials. Such parameterizations are easy to generate, as already done in our experiments in Section VI.

APPENDIX B

STABILITY PROOF FOR THE SLICING PHASE

In the slicing phase, hybrid force/position control is applied to regulate the cutting velocity in the horizontal direction as well as the contact force in the vertical direction. The following closed-loop system equation is obtained by subtracting the dynamics (38) from the controller (40):

$$ML_c^\dagger(\alpha_1, 0, \alpha_2)^\top - J_c^\top(0, \alpha_3, 0)^\top = \mathbf{0}, \quad (58)$$

where the error items are

$$\begin{aligned}
\alpha_1 &= \ddot{c}_{xe} + k_{v|c} \dot{c}_{xe} + k_{p|c} c_{xe} + k_{i|c} \int c_{xe} dt, \\
\alpha_2 &= \ddot{\psi}_e + k_{v|c} \dot{\psi}_e + k_{p|c} \psi_e + k_{i|c} \int \psi_e dt, \\
\alpha_3 &= f_{ye} + k_{fi} \int f_{ye} dt.
\end{aligned}$$

Multiplying $(\alpha_1, 0, \alpha_2)(L_c^\dagger)^\top$ with both sides of (58):

$$\begin{aligned}
&(\alpha_1, 0, \alpha_2)(L_c^\dagger)^\top ML_c^\dagger(\alpha_1, 0, \alpha_2)^\top \\
&\quad - (\alpha_1, 0, \alpha_2)(L_c^\dagger)^\top J_c^\top(0, \alpha_3, 0)^\top = 0. \quad (59)
\end{aligned}$$

We rewrite the subtracted term on the left hand side below:

$$\begin{aligned}
&(\alpha_1, 0, \alpha_2)(L_c^\dagger)^\top J_c^\top(0, \alpha_3, 0)^\top \\
&= (\alpha_1, 0, \alpha_2)(J_c L_c^\dagger)^\top(0, \alpha_3, 0)^\top \\
&= (\alpha_1, 0, \alpha_2) \left(L_c L_c^\dagger - \left(R(\psi) \frac{\partial}{\partial \boldsymbol{\theta}} (\boldsymbol{\beta}'(u(\boldsymbol{\theta}))) \right) L_c^\dagger \right)^\top \begin{pmatrix} 0 \\ \alpha_3 \\ 0 \end{pmatrix}, \quad (60)
\end{aligned}$$

where the last step substituted (36) in. Since $L_c L_c^\dagger = I_3$, we have

$$\begin{aligned}
&(\alpha_1, 0, \alpha_2)(L_c L_c^\dagger)^\top(0, \alpha_3, 0)^\top \\
&= (\alpha_1, 0, \alpha_2) I_3(0, \alpha_3, 0)^\top \\
&= 0. \quad (61)
\end{aligned}$$

With the rotation matrix

$$R(\psi) = \begin{pmatrix} \cos \psi & -\sin \psi \\ \sin \psi & \cos \psi \end{pmatrix}, \quad (62)$$

we have

$$\begin{aligned}
&R(\psi) \frac{\partial}{\partial \boldsymbol{\theta}} (\boldsymbol{\beta}'(u(\boldsymbol{\theta}))) \\
&= R(\psi) \frac{d\boldsymbol{\beta}'}{du} \nabla u(\boldsymbol{\theta}) \quad \text{by (37)} \\
&= \begin{pmatrix} (\cos \psi, -\sin \psi) \frac{d\boldsymbol{\beta}'}{du} \nabla u(\boldsymbol{\theta}) \\ \mathbf{0} \end{pmatrix}. \quad \text{by (29)} \quad (63)
\end{aligned}$$

Now we substitute both (61) and (63) into equation (60):

$$\begin{aligned}
&(\alpha_1, 0, \alpha_2)(L_c^\dagger)^\top J_c^\top(0, \alpha_3, 0)^\top \\
&= -(\alpha_1, 0, \alpha_2)(L_c^\dagger)^\top \begin{pmatrix} (\cos \psi, -\sin \psi) \frac{d\boldsymbol{\beta}'}{du} \nabla u(\boldsymbol{\theta}) \\ \mathbf{0} \end{pmatrix}^\top \begin{pmatrix} 0 \\ \alpha_3 \\ 0 \end{pmatrix} \\
&= -(\alpha_1, 0, \alpha_2)(L_c^\dagger)^\top \mathbf{0} \\
&= 0. \quad (64)
\end{aligned}$$

Consequently, equation (59) reduces to

$$(\alpha_1, 0, \alpha_2)(L_c^\dagger)^\top ML_c^\dagger(\alpha_1, 0, \alpha_2)^\top = 0.$$

Since the inertia matrix M is positive definite, the above equation holds if and only if $L_c^\dagger(\alpha_1, 0, \alpha_2)^\top = 0$, which implies $\alpha_1 = 0$ and $\alpha_2 = 0$ because L_c^\dagger has independent columns as a result of L_c 's full row rank. Convergences of the errors c_{xe} and ψ_e to zero are guaranteed by choosing the controller gains based on the third order LTI system stability, which requires $k_{p|a}, k_{i|a}, k_{v|a} > 0$ and $k_{p|a} k_{v|a} > k_{i|a}$.

Substituting $\alpha_1 = 0$ and $\alpha_2 = 0$ into (58), we have $(0, \alpha_3, 0) J_c = 0$, which leads to

$$\alpha_3 \frac{\partial \beta_{\theta,y}}{\partial \boldsymbol{\theta}} = \mathbf{0}$$

by (34) and $\boldsymbol{\beta}_\theta = (\beta_{\theta,x}, \beta_{\theta,y})^\top$. Since the partial derivative vector $\partial \beta_{\theta,y} / \partial \boldsymbol{\theta}$ does not vanish, the above equation implies

$$\alpha_3 = f_{ye} + k_{fi} \int f_{ye} dt = 0.$$

This is a first order LTI system whose stability can be ensured by a positive value of the gain k_{fi} .

REFERENCES

- [1] S. Srinivasa, D. Berenson, M. Cakmak, A. Collet, M. R. Dogar, A. D. Dragan, R. A. Knepper, T. D. Niemuller, K. Strabala, J. V. Weghe, and J. Ziegler, "Herb 2.0: Lessons learned from developing a mobile manipulator for the home," *Proc. IEEE*, vol. 100, no. 8, pp. 2410–2428, Jun. 2012.
- [2] H. Iwata and S. Sugeno, "Design of human symbiotic robot TWENDY-ONE," in *Proc. IEEE Int. Conf. Robot. Autom.*, May. 2009, pp. 580–586.
- [3] M. Bleetz, U. Klank, I. Kresse, A. Maldonado, M. Mösenlechner, D. Pangercic, T. Rühr, and M. Tenorth, "Robotic roommates making pancakes," in *Proc. IEEE-RAS Int. Conf. Humanoid Robots*, Oct. 2011, pp. 529–536.
- [4] "Watch a Robot Make a Burger at Creator Restaurant San Francisco." [Online]. Available: <https://www.youtube.com/watch?v=5TBnwh7U1AU>
- [5] "World's First Robotic Kitchen Launched." [Online]. Available: <https://www.prnewswire.com/news-releases/worlds-first-robotic-kitchen-launched-301206400.html>
- [6] P. Y. Chua, T. Ihschner, and D. G. Caldwell, "Robotic manipulation of food products a review," *Ind. Robot*, vol. 30, no. 4, pp. 345–354, Aug. 2003.
- [7] Z. Wang, S. Hirai, and S. Kawamura, "Challenges and opportunities in robotic food handling: a review," *Front. Robot. AI*, vol. 8, pp. 1–12, Jan. 2022.
- [8] B. Zhang, Y. Xie, J. Zhou, K. Wang, and Z. Zhang, "State-of-the-art robotic grippers grasping and control strategies as well as their applications in agricultural robots: A review," *Comput. Electron. Agricult.*, vol. 177, Oct. 2020.
- [9] T. Bhattacharjee, G. Lee, H. Song, and S. S. Srinivasa, "Towards Robotic Feeding: Role of Haptics in Fork-Based Food Manipulation," *IEEE Robot. Autom. Letters*, vol. 4, no. 2, pp. 1485–1492, Apr. 2019.
- [10] K. Junge, J. Hughes, T. G. Thuruthel, and F. Iida, "Improving robotic cooking using batch bayesian optimization," *IEEE Robot. Autom. Letters*, vol. 5, no. 2, pp. 760–765, Jan. 2020.
- [11] "Meat Cutting Robot." [Online]. Available: <https://www.clkgmbh.de/en/automatic-meat-cutting-line-calculation/>
- [12] "Automatic Chicken Breast Deboning Robot." [Online]. Available: https://www.youtube.com/watch?v=UjFWrv_IAw
- [13] "How It Works: The Robotic Chicken Butcher." [Online]. Available: <https://www.popsci.com/technology/article/2013-03/robotic-chicken-butcher/>
- [14] "Modern Food Processing Technology with Cool Automatic Machines That Are At Another Level Part 18." [Online]. Available: <https://www.youtube.com/watch?v=ImANsZIZuKQ>
- [15] "WebstaurantStore." [Online]. Available: <https://www.webstaurantstore.com>
- [16] A. S. Saada, *Elasticity: Theory and Applications*. Malabar, FL: Krieger Publishing Company, 1993.
- [17] V. V. Novozhilov, *Foundations of the Nonlinear Theory of Elasticity*. Rochester, NY: Graylock, 1953; Dover, 1999.
- [18] T. L. Anderson, *Fracture Mechanics: Fundamentals and Applications*, 3rd ed. Boca Raton, FL: CRC Press, 2005.
- [19] M. A. Peshkin and A. C. Sanderson, "Minimization of energy in quasistatic manipulation," *Proc. IEEE Int. Conf. Robot. Autom.*, Apr. 1988, pp. 421–426.
- [20] J. Trinkle and D. C. Zeng, "Prediction of the quasistatic planar motion of a contacted rigid body," *IEEE Trans. Robot. and Autom.*, vol. 11, no. 2, pp. 230–246, Apr. 1995.
- [21] X. Mu, Y. Xue, and Y.-B. Jia, "Robotic cutting: Mechanics and control of knife motion," in *Proc. IEEE Int. Conf. Robot. Autom.*, May. 2019, pp. 3066–3072.
- [22] T. Atkins, *The Science and Engineering of Cutting*. Oxford, UK: Elsevier, 2009.
- [23] A. G. Atkins, "Toughness and cutting: A new way of simultaneously determining ductile fracture toughness and strength," *Engr. Fracture Mechanics*, vol. 72, no. 6, pp. 849–860, Apr. 2004.
- [24] C. Gokgol, C. Basdogan, and D. Canadinc, "Estimation of fracture toughness of liver tissue: Experiments and validation," *Medical Engr. Phy.*, vol. 34, no. 7, pp. 882–891, Sep. 2012.
- [25] T. Chanthasopeephan, J. P. Desai, and A. C. W. Lau, "Measuring forces in liver cutting: New equipment and experimental results," *Ann. Biomed. Eng.*, vol. 31, no. 11, pp. 1372–1382, Dec. 2003.
- [26] A. G. Atkins and X. Xu, "Slicing of soft flexible solids with industrial applications," *Int. J. Mech. Sci.*, vol. 47, no. 4, pp. 479–492, Apr. 2005.
- [27] A. G. Atkins, X. Xu, and G. Jeronimidis, "Cutting, by 'pressing and slicing,' of thin floppy slices of materials illustrated by experiments on cheddar cheese and salami," *J. Materials Sci.*, vol. 39, no. 8, pp. 2761–2766, Apr. 2004.
- [28] E. Reysat, T. Tallinen, M. Le Merrer, and L. Mahadevan, "Slicing softly with shear," *Phys. Rev. Lett.*, vol. 109, no. 24, p. 244301, Dec. 2012.
- [29] P. P. Jamdagni and Y.-B. Jia, "Robotic slicing of fruits and vegetables: modeling the effects of fracture toughness and knife geometry," in *Proc. IEEE Int. Conf. Robot. Autom.*, May. 2021, pp. 6607–6613.
- [30] D. Bielser, P. Glardon, M. Teschner, and M. Gross, "A state machine for real-time cutting of tetrahedral meshes," *Graphical Models*, vol. 66, no. 6, pp. 398–417, Nov. 2004.
- [31] N. Molino, Z. Bao, and R. Fedkiw, "A virtual node algorithm for changing mesh topology during simulation," *ACM Transactions on Graphics*, vol. 23, no. 3, pp. 385–392, Jan. 2004.
- [32] I. Berndt, R. Torchelsen and A. Maciel, "Efficient surgical cutting with position-based dynamics," in *IEEE Computer Graphics and Applications*, vol. 37, no. 3, pp. 24–31, May-Jun. 2017.
- [33] J. Wolper, Y. Fang, M. Li, J. Lu, M. Gao, and C. Jiang, "Cdmpm: continuum damage material point methods for dynamic fracture animation," *ACM Transactions on Graphics*, vol. 38, no. 4, pp. 1–15, Jul. 2019.
- [34] D. Zhou, M. R. Claffee, K.-M. Lee, and G. V. McMurray, "Cutting, 'by pressing and slicing', applied to robotic cutting bio-materials, Part I: Modeling of stress distribution," in *Proc. IEEE Int. Conf. Robot. Autom.*, May. 2006, pp. 2896–2901.
- [35] D. Zhou, M. R. Claffee, K.-M. Lee, and G. V. McMurray, "Cutting, 'by pressing and slicing', applied to robotic cutting bio-materials, Part II: Force during slicing and pressing cuts," in *Proc. IEEE Int. Conf. Robot. Autom.*, May. 2006, pp. 2256–2261.
- [36] D. Zhou and G. McMurray, "Modeling of blade sharpness and compression cut of biomaterials," *Robotica*, vol. 28, no. 2, pp. 311–319, Mar. 2010.
- [37] V. Chial, S. Greenish, and A. M. Okamura, "On the display of haptic recordings for cutting biological tissues," in *HAPTICS*, Mar. 2002, pp. 80–87.
- [38] T. Chanthasopeephan, J. P. Desai, and A. C. W. Lau, "Modeling soft-tissue deformation prior to cutting for surgical simulation: Finite analysis and study of cutting parameters," *IEEE Trans. Biomed. Engr.*, vol. 54, no. 3, pp. 349–359, February. 2007.
- [39] L. Bogoni and R. Bajcsy, "Interactive Recognition and Representation of Functionality," *Computer Vision and Image Understanding*, vol. 62, no. 2, pp. 194–214, Sep. 1995.
- [40] M. Khadem, C. Rossa, R. S. Sloboda, N. Usmani, and M. Tavakoli, "Mechanics of tissue cutting during needle insertion in biological tissue," *IEEE Robot. Autom. Letters*, vol. 1, no. 2, pp. 800–807, Jul. 2016.
- [41] B. Thananjeyan, A. Garg, S. Krishnan, C. Chen, L. Miller, and K. Goldberg, "Multilateral surgical pattern cutting in 2D orthotropic gauze with deep reinforcement learning policies for tensioning," in *Proc. IEEE Int. Conf. Robot. Autom.*, May. 2017, pp. 2371–2378.
- [42] Z. Jiang, X. Qi, Y. Sun, Y. Hu, G. Zahnd, and J. Zhang, "Cutting depth monitoring based on milling force for robot-assisted laminectomy," *IEEE Trans. Autom. Sci. Eng.*, vol. 17, no. 1, pp. 2–14, Jan. 2020.
- [43] L. Han, H. Wang, Z. Liu, W. Chen, and X. Zhang, "Vision-based cutting control of deformable objects with surface tracking," *IEEE/ASME Trans. Mechatronics*, vol. 26, no. 4, pp. 2016–2026, Aug. 2021.
- [44] B. Takabi and B. L. Tai, "A review of cutting mechanics and modeling techniques for biological materials," *Medical Engr. Phys.*, vol. 45, pp. 1–14, Jul. 2017.
- [45] G. Zeng and A. Hemami, "An adaptive control strategy for robotic cutting," in *Proc. IEEE Int. Conf. Robot. Autom.*, Apr. 1997, pp. 22–27.
- [46] S. Jung and T. C. Hsia, "Adaptive force tracking impedance control of robot for cutting nonhomogeneous workpiece," in *Proc. IEEE Int. Conf. Robot. Autom.*, May. 1999, pp. 1800–1805.
- [47] P. Long, W. Khalil, and P. Martinet, "Force/vision control for robotic cutting of soft materials," in *Proc. IEEE/RSJ Int. Conf. Intell. Robots Syst.*, Sep. 2014, pp. 4716–4721.
- [48] P. Long, W. Khalil, and P. Martinet, "Modeling and control of a meat-cutting robotic cell," in *Proc. Int. Conf. Advanced Robot.*, Nov. 2013, pp. 1–6.
- [49] A. P. Hu, J. Bailey, M. Matthews, G. McMurray, and W. Daley, "Intelligent automation of bird deboning," in *Proc. IEEE/ASME Int. Conf. Adv. Intell. Mechatronics*, Jul. 2012, pp. 286–291.

- [50] A. Yamaguchi and C. G. Atkeson, "Combining finger vision and optical tactile sensing: Reducing and handling errors while cutting vegetables," in *Proc. IEEE-RAS Int. Conf. Humanoid Robots*, Nov. 2016, pp. 1045–1051.
- [51] R. M. Murray, Z. Li, and S. S. Sastry, *A Mathematical Introduction to Robotic Manipulation*. Boca Raton, FL: CRC Press, 1994.
- [52] N. Hogan, "Impedance control: An approach to manipulation: Parts I–III," *ASME. J. Dyn. Sys., Meas., Control*, vol. 107, no. 1, pp. 1–24, Mar. 1985.
- [53] P. Song, Y. Yu, and X. Zhang, "A tutorial survey and comparison of impedance control on robotic manipulation," *Robotica*, vol. 37, no. 5, pp. 801–836, Jan. 2019.
- [54] M. T. Mason, "Compliance and force control for computer controlled manipulators," *IEEE Trans. Syst., Man, and Cybern.*, vol. 11, no. 6, pp. 418–432, Jun. 1981.
- [55] M. H. Raibert and J. J. Craig, "Hybrid position/force control of manipulators," *ASME. J. Dyn. Sys., Meas., Control*, vol. 103, no. 2, pp. 126–133, Jun. 1981.
- [56] T.-J. Tarn, Y. Wu, N. Xi, and A. Isidori, "Force regulation and contact transition control," *IEEE Control Syst. Mag.*, vol. 16, no. 1, pp. 32–40, Feb. 1996.
- [57] O. Khatib, "A unified approach for motion and force control of robot manipulators: The operational space formulation," *IEEE J. Robot. Autom.*, vol. 3, no. 1, pp. 43–53, Feb. 1987.
- [58] F. L. Lewis, D. M. Dawson, and C. T. Abdallah, *Robot Manipulator Control: Theory and Practice*, 2nd ed. New York, NY: Marcel Dekker, Inc., 2004.
- [59] M. C. Gemic, and A. Saxena, "Learning haptic representation for manipulating deformable food objects," in *Proc. IEEE/RSJ Int. Conf. Intell. Robots Syst.*, Sep. 2014, pp. 638–645.
- [60] I. Lenz, R. Knepper, and A. Saxena, "DeepMPC: Learning deep latent features for model predictive control," in *Robotics: Science and Systems*, Jul. 2015.
- [61] A. Bemporad, "Model predictive control design: new trends and tools," in *Proc. IEEE Conf. Decis. Control*, Dec. 2006, pp. 6678–6683.
- [62] I. Mitsioni, Y. Karayiannidis, J. A. Stork, and D. Kragic, "Data-driven model predictive control for the contact-rich task of food cutting," in *Proc. IEEE-RAS Int. Conf. Humanoid Robots.*, Oct. 2019, pp. 244–250.
- [63] I. Mitsioni, Y. Karayiannidis, and D. Kragic, "Modelling and Learning Dynamics for Robotic Food-Cutting," in *Proc. IEEE-RAS Int. Conf. Automation Science and Engineering*, Aug. 2021, pp. 1194–1200.
- [64] K. Zhang, M. Sharma, M. Veloso, and O. Kroemer, "Leveraging multimodal haptic sensory data for robust cutting," in *Proc. IEEE-RAS Int. Conf. Humanoid Robots*, Oct. 2019, pp. 409–416.
- [65] E. Heiden, M. Macklin, Y. Narang, D. Fox, A. Garg, and F. Ramos, "IDiSECT: A Differentiable Simulation Engine for Autonomous Robotic Cutting," in *Robotics: Science and Systems*, Jul. 2021.
- [66] A. Straižys, M. Burke, and S. Ramamoorthy, "Surfing on an uncertain edge: Precision cutting of soft tissue using torque-based medium classification," in *Proc. IEEE Int. Conf. Robot. Autom.*, May. 2020, pp. 4623–4629.
- [67] Z. Xu, Z. Xian, X. Lin, C. Chi, Z. Huang, C. Gan, and S. Song, "RoboNinja: Learning an adaptive cutting policy for multi-material objects," arXiv:2302.11553v1. [Online]. Available: <https://arxiv.org/abs/2302.11553>.
- [68] D. E. Whitney, "The Mathematics of Coordinated Control of Prosthetic Arms and Manipulators," *ASME. J. Dyn. Sys., Meas., Control*, vol. 94, no. 4, pp. 303–309, Dec. 1972.
- [69] Y. Nakamura and H. Hanafusa, "Inverse Kinematic Solutions With Singularity Robustness for Robot Manipulator Control," *ASME. J. Dyn. Sys., Meas., Control*, vol. 108, no. 3, pp. 163–171, Sep. 1986.
- [70] B. Siciliano, "Kinematic control of redundant robot manipulators: A tutorial," *J. Intell. Robot. Syst.*, vol. 3, no. 3, pp. 201–222, Sep. 1990.
- [71] J. M. Hollerbach and K. C. Suh, "Redundancy resolution of manipulators through torque optimization," *IEEE Trans. Robot. Autom.*, vol. 3, no. 4, pp. 308–316, Aug. 1987.
- [72] A. Dietrich, C. Ott, and A. Albu-Schäffer, "An overview of null space projections for redundant, torque-controlled robots," *Int. J. Robot. Res.*, vol. 34, no. 11, pp. 1385–1400, Mar. 2015.
- [73] R. C. Dorf and R. H. Bishop, *Modern Control Systems*. Hoboken, NJ: Prentice Hall Inc., 2001.
- [74] T. Kailath, *Linear Systems*. Englewood Cliffs, NJ: Prentice Hall, 1980.
- [75] S. P. Boyd and L. Vandenberghe, *Convex Optimization*. Cambridge, U.K.: Cambridge Univ. Press, 2004.
- [76] "WAM Arm Inertial Specifications." [Online]. Available: http://web.barett.com/support/WAM_Documentation/WAM_InertialSpecifications_AC-02.pdf
- [77] L. Villani and J. De Schutter, "Force control," in *Handbook of Robotics*, B. Siciliano and O. Khatib, Eds. New York, NY, USA: Springer-Verlag, 2008.
- [78] X. Mu and Y.-B. Jia, "Physical Property Estimation and Knife Trajectory Optimization During Robotic Cutting," in *Proc. IEEE Int. Conf. Robot. Autom.*, May. 2022, pp. 2700–2706.
- [79] P. P. Jamdagni and Y.-B. Jia, "Robotic cutting of solids based fracture mechanics and FEM," in *Proc. IEEE/RSJ Int. Conf. Intell. Robots Syst.*, Nov. 2019, pp. 8246–8251.
- [80] A. R. Hirakawa and A. Kawamura, "Trajectory planning of redundant manipulators for minimum energy consumption without matrix inversion," in *Proc. IEEE Int. Conf. Robot. Autom.*, Apr. 1997, pp. 2415–2420.
- [81] O. Wigström, B. Lennartson, A. Vergnano, and C. Breitholtz, "High-level scheduling of energy optimal trajectories," *IEEE Trans. Autom. Sci. Eng.*, vol. 10, no. 1, pp. 57–64, Jan. 2013.
- [82] O. Khatib, "Dynamic control of manipulators in operational space," in *Proc. 6th IFTOMM Congress on Theory of Machines and Mechanisms*, Dec. 1983, pp. 1123–1131.



Xiaoqian Mu received the B.S. degree in automation from the University of Science and Technology of China, Hefei, China, in 2015, and the Ph.D. degree in computer science from Iowa State University, Ames, IA, USA, in 2021.

Since 2021, she has been a Robotics Engineer with Aescap Inc., New York, NY, USA, where she currently works on control system design and controller development for robot manipulation applications. Her research interests include robotic control, dexterous cutting, and impulsive manipulation.

Dr. Mu has received the Robert Stewart Early Research Recognition Award for her research on dexterous robotic cutting, in 2019.



Yuechuan Xue (Student Member, IEEE) received the B.S. degree in physics from the University of Science and Technology of China, Hefei, China, in 2016, and the Ph.D. degree in computer science from Iowa State University, Ames, IA, USA, in 2022.

He is an applied scientist with Amazon, Cambridge, MA, USA, where he works on motion planning for warehouse robotics. His research interests include motion planning and control for dexterous arm-hand systems with uncertainty.

Dr. Xue received the Robert Stewart Early Research Recognition Award for his research on robotic hand manipulation, in 2018.



Yan-Bin Jia (Senior Member, IEEE) received the B.S. degree in computer science from the University of Science and Technology of China, Hefei, China, in 1988, and the M.S. and Ph.D. degrees in robotics from Carnegie Mellon University, Pittsburgh, PA, USA, in 1993 and 1997, respectively.

He is currently a Professor with the Department of Computer Science, Iowa State University, Ames, IA, USA. His research interests include dynamic finger gaiting, dexterous cutting, impact mechanics, impulsive manipulation, deformable modeling and

grasping, pose and motion estimation, and tactile shape recognition and reconstruction.

Dr. Jia has received the US National Science Foundation Faculty Early Career Development Award in 2002. He was an Associate Editor of the IEEE Transactions on Robotics from 2017 to 2021 and Automation Science and Engineering from 2008–2011, and a Co-Editor of a Special Issue on Tactile Presence of the International Journal of Robotics Research in 2000.